This is to certify that the
thesis entitled

Independent Component Analysis for Enhanced Feature Extraction in NDE Applications

presented by

Byung Hyuk Shin

has been accepted towards fulfillment
of the requirements for the

M.S. degree in Electrical Engineering

Major Professor's Signature

June 3, 2004

Date

Independent Component Analysis for Enhanced Feature Extraction from Non-destructive Evaluation

By

Byung Hyuk Shin

A THESIS

Submitted to
Michigan State University
in partial fulfillment of the requirements
for the degree of

MASTER OF SCIENCE

Department of Electrical and Computer Engineering

2004

ABSTRACT

Independent Component Analysis for Enhanced Feature Extraction in NDE Applications

By

Byung Hyuk Shin

In this thesis, independent component analysis (ICA) is proposed for enhancing flaw information in eddy current nondestructive evaluation (NDE). ICA provides a method for representing data as weighted combination of independent components and higher-order statistics of the data is used to minimize the dependence between the components of the system output. Multi-frequency eddy current testing is a widely used NDE method in situations where the defect signal is corrupted by noise and contributions from external supports that makes the analysis challenging. ICA, along with an affine transformation as a preprocessing stage, is shown to extract the defect signal from a combination of defect, support and noise signals, while improving the SNR.

ACKNOWLEDGEMENTS

I would like to express my deep gratitude to major professor Dr. Lalita Udpa for her kind guidance, support, and encouragement during my graduate study. I also thank her for taking time to revise my thesis. I would sincerely like to thank Dr. Satish Udpa and Dr. Pradeep Ramuhalli for their technical support and invaluable advice through the project. I wish to express my special thanks to the members of NDEL at Michigan State University for sharing their knowledge and time.

My deep gratitude goes to my parents their warm love, support, and encouragement during my study in East Lansing. I am also thankful to all my friends in Korea and MSU for their suggestions and kind help during my study.

TABLE OF CONTENTS

LIST OF FIGURES

LIST OF TABLES

1. INTRODUCTION

Steam generators (SG) are heat exchange units in nuclear power plants (NPP) [1]. The function of the steam generator is to transfer the heat generated in the primary loop to a mixture of water and steam circulating outside the tube. The water around the tubes absorbs the heat and vaporizes into steam which is used to run the turbines. Ferromagnetic support plates in the steam generator located at periodic intervals are used to anchor the tubes. The steam generator tubes and support plates when exposed to extreme environments such as high temperature and pressure can result in corrosion products which are deposited in the crevice between tubes and support plates. This, in turn, leads to denting, thinning and cracking of the tube. When cracking occurs in the tubes, radioactive primary water can leak and contaminate the water and steam used to drive the turbines. Hence, it is very critical to find small flaws in the SG tubes before they develop into a propagating crack.

It is critical that there is no leakage of fluid from the primary loop into the secondary loop. However, the harsh environmental conditions cause the tubes in the SG unit to be subjected to various types of degradation mechanisms such as mechanical wear between tube and support plate, outer diameter stress corrosion cracking (ODSCC), pitting, volumetric changes, primary water stress corrosion cracking (PWSCC) and inter granular attack (IGA), all of which result in tube thinning and cracking. Since the outage of a NPP costs almost $500,000 a day, there is a strong motivation to develop a reliable method to assess the safety of the unit. The steam generator tubes are inspected periodically for cracks, and degradation.

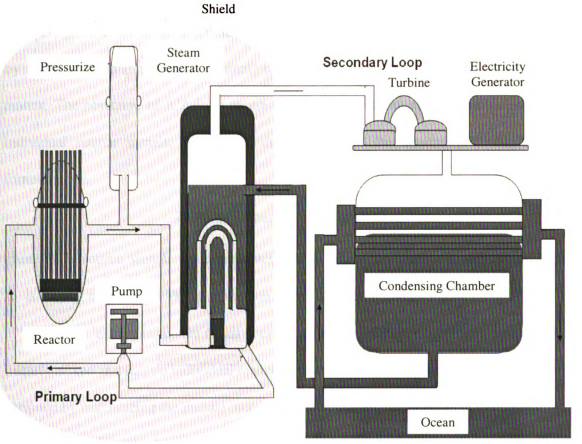

Figure1.1 Schematic of a Nuclear Power Plant

Eddy current technique [2,3] is a widely used practical tool for inspecting SG tubes. Although the measured eddy current data contain information related to defects, it is sometimes corrupted by noise and contribution from external support plates that make the analysis challenging. This problem is usually solved by means of a mixing algorithm [4] implemented using multi-frequency eddy current data where a signal at a low excitation frequency is transformed to the corresponding signal at high frequency and the transformed signal is subtracted from the measured high frequency signal to suppress the tube support plate (TSP) contribution.

This thesis investigates the use of Independent Component Analysis (ICA) to separate out the signals due to defects and tube supports from noise. The measured data is modeled by a combination (linear or non-linear) of the sources that is represented using a mixing matrix. The objective of ICA is to invert the unknown mixing system and to estimate the individual source signals. In general, the mixing and the separation problem can be formulated as

$$\hat{\mathbf{s}} = \mathbf{W}\mathbf{x} \quad \text{where} \quad \mathbf{x} = \mathbf{A}\mathbf{s} \tag{1.1}$$

where $\mathbf{s}$ is source signal, $\mathbf{x}$ is measurement, $\hat{\mathbf{s}}$ represents the estimated source signal. $\mathbf{A}$ is mixing matrix and $\mathbf{W}$ is separation matrix that is the inverse of $\mathbf{A}$.

Under the assumptions that (i) all sources are mutually independent, (ii) the signals are linearly mixed and (iii) no individual source signal is Gaussian, the separation system can be obtained by maximizing the mutual independence between components.

ICA was originally developed to solve the cocktail party problem of extracting speech signals of individuals from data obtained by recording sounds from a roomful of people. It was originally addressed as the problem of blind source separation by Christian Jutten and Jeanny Herault in the early of 1980`s [5, 6]. In the context of blind source separation, the inverse problem has been well studied and many algorithms have been developed depending on the nature of the mixing model. The problem of blind source separation is more difficult since the mixing matrix is unknown. The only assumption made by Jutten and Herault was the independence of the source signals. A fast and efficient algorithm was required and Bell and Sejnowski obtained the result based on infomax approach to ICA [7]. S. Amari soon realized that the infomax ICA algorithm could be improved by using the natural gradient, which multiplies the gradient of the feed forward weight matrix by a positive definite matrix

and makes it converge faster by eliminating the matrix inversion [8]. This allowed infomax ICA algorithm to be practical for various problems in the real world. In 1998, Te-Won Lee, Mark Girolami and Sejnowski developed the extended version of infomax ICA algorithm that is suitable for general non-Gaussian signals [9]. Finnish researchers, A. Hyvärinen and E. Oja, developed the fast and robust metric known as fast ICA algorithm for fixed-point data [10, 11].

This thesis is organized into 6 chapters. Chapter 2 describes the physical principles of eddy current technique and multi-frequency eddy current (MFEC) data while Chapter 3 presents the primary approach proposed in this thesis, namely independent component analysis (ICA). Chapter 4 introduces the application of ICA to ECT data and finite element method (FEM) for NDE. The simulation results are presented and discussed in Chapter 5. Conclusions and directions for future work are given in Chapters 6.

2. EDDY CURRENT TECHNIQUE

2.1. Principles of Eddy Current Technique (ECT)

Eddy Current Method is a widely used nondestructive testing technique in nuclear, aerospace, power, transport, petroleum and other industries to inspect conducting samples for detection and characterization of defects, corrosion and other variations. ECT is based on electromagnetic induction and hence direct electrical contact with the material is not required. ECT is widely used largely, because it is a non-contact method and can detect surface and sub-surface defects (fatigue cracks, stress corrosion cracks) with high-speed, accuracy and reliability.

ECT is principally based on the Maxwell-Ampere law and Faraday's law of electromagnetic induction. When a coil is excited by alternating currents, a time-varying magnetic field is set up in accordance with the Maxwell-Ampere law [12].

$$\oint_C \mathbf{H} \bullet d\vec{l} = \iint_S \mathbf{J} \bullet d\vec{s} \tag{2.1}$$

When the coil is brought close to a conducting material, the primary field associated with the coil induces EMF in the medium according to the Maxwell-Faraday law.

$$\oint_C \mathbf{E} \bullet d\vec{l} = -\iint_S \frac{\partial \mathbf{B}}{\partial t} \bullet d\vec{s} \tag{2.2}$$

which produces eddy currents that flows in closed paths and it is shown in Figure 2.1.

According to Lenz's law, the EMF and induced currents are directed so as to oppose the change that produces them. The magnetic field set up by the induced eddy current opposes the primary magnetic field associated with the coil. When the test specimen is nonferromagnetic the net flux linkages of the coil decreases which in turn decreases the inductance of the coil. Accompanying the decrease in the inductance is an increase in

resistance of the coil since the eddy current losses incurred in the specimen has to be met by the source of primary excitation. The presence of discontinuity in the material results in the different magnetic flux linkages. Therefore, the changes in coil impedance due to the presence of flaws can be analyzed to estimate the surface properties of the specimen [13].

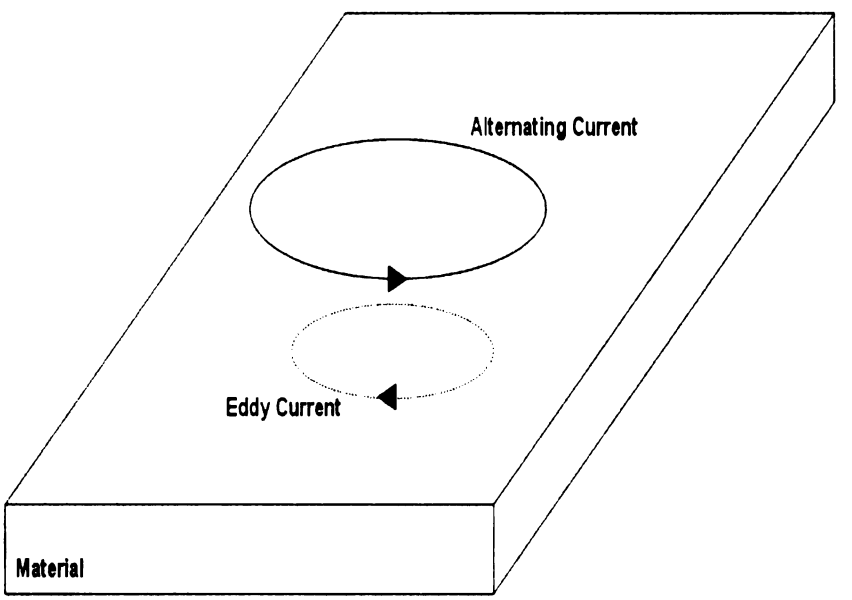

Figure 2.1 Eddy Current Principle

Eddy current signals are displayed as horizontal and vertical channel data of the complex impedance in the impedance plane and trajectory. The eddy current probe data can be measured using an AC bridge as shown in Figure 2.2.

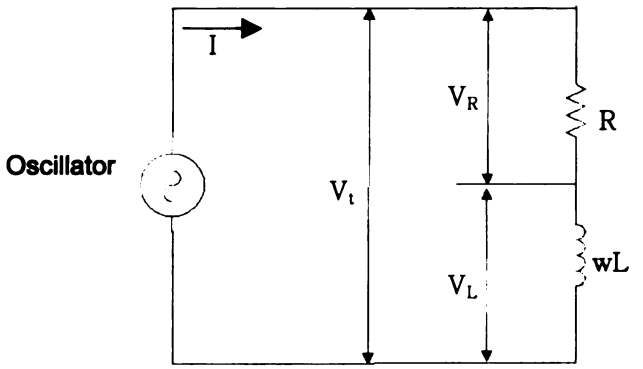

Figure 2.2 Simplified Model of ECT Probe

In a direct current (DC) circuit, current and voltage can be represented by the magnitude. However, the analysis of alternating current (AC) circuit is more complicated. Since the magnitude of current and voltage vary with time, not only the magnitude information but the phase information must be taken into account. Assume that a resistor and inductor are connected in series with an oscillator (Figure 2.2). This is a typical AC circuit and can be considered to be a simplified model of probe. The inductor models the reactive part of the coil while the resistor models both coil wire and cable resistance. For this circuit, the voltage across the inductor (V_L) leads the current (I) by 90° while voltage across the resistor (V_R) has the same phase with the current. Therefore, the current can serve as a point of reference. As a result, the voltage across the inductor leads the voltage across the resistor by 90°. The voltage across the resistor and inductor (V_L) leads the current (or the voltage across the resistor) by an angle less than 90°.

To evaluate the total voltage (V_T), we add the voltage across the resistor (V_R) and the inductor (V_L).

$$
\begin{aligned}
V_T &= V_R + V_L \\
&= I(R + jwL) \\
&= IRsin(wt + 0) + jwLsin(wt + \pi/2)
\end{aligned} \tag{2.3}
$$

Hence, the impedance is represented as

$$Z = \frac{V_T}{I} = Rsin(wt) + jwLsin(wt + \pi/2) \tag{2.4}$$

The two terms in the last equation (2.3) contain the amplitude and phase shift. Hence, they can be represented by phasors. The amplitude of the first term is R and the phase shift is 0 while the amplitude of the second term is wL and the phase shift is $\pi/2$.

2.2. The Eddy Current Phenomenon

The governing equation for eddy current phenomenon can be derived from Maxwell`s equations [12, 14]. In differential form, the Maxwell`s equations can be written as

$$\nabla \times \mathbf{E} = -\frac{\partial \mathbf{B}}{\partial t} \tag{2.5}$$

$$\nabla \times \mathbf{H} = \mathbf{J} + \frac{\partial \mathbf{D}}{\partial t} \tag{2.6}$$

$$\nabla \bullet \mathbf{B} = 0 \tag{2.7}$$

$$\nabla \bullet \mathbf{D} = \rho \tag{2.8}$$

and the constitutive relations for isotropic, linear and homogeneous medium are

$$\mathbf{B} = \mu \mathbf{H} \tag{2.9}$$

$$\mathbf{D} = \varepsilon \mathbf{E} \tag{2.10}$$

$$\mathbf{J} = \sigma \mathbf{E} \tag{2.11}$$

where

ε is the electric permittivity (farads/m)

μ is the magnetic permeability (Henry/m)

σ is the electric conductivity (mhos/m)

Since $\nabla \bullet \mathbf{B} = 0$, $\mathbf{B}$ can be expressed as the curl of the vector magnetic potential $\mathbf{A}$ given by

$$\mathbf{B} = \nabla \times \mathbf{A} \tag{2.12}$$

Substituting for $\mathbf{B}$ in equation (2.5)

$$\nabla \times \mathbf{E} = -\nabla \times \frac{\partial \mathbf{A}}{\partial t}$$

$$\text{or} \quad \nabla \times \left(\mathbf{E} + \frac{\partial \mathbf{A}}{\partial t} \right) = 0 \tag{2.13}$$

Using the vector identities we express

$$\mathbf{E} + \frac{\partial \mathbf{A}}{\partial t} = -\nabla \varphi \tag{2.14}$$

where φ is the scalar electric potential.

Substituting equation (2.11) in equation (2.14) we have

$$\mathbf{J} = -\left(\sigma \frac{\partial \mathbf{A}}{\partial t} + \sigma \nabla \phi \right) = -\sigma \frac{\partial \mathbf{A}}{\partial t} + \mathbf{J_S} \tag{2.15}$$

where $\mathbf{J_S} = -\sigma \nabla \phi$ is the source current density and $\sigma \frac{\partial \mathbf{A}}{\partial t}$ is the induced eddy current density.

At the excitation frequencies for eddy current testing the displacement current $\frac{\partial \mathbf{D}}{\partial t}$ in equation (2.6) is negligibly small incomparison with the conduction current density $\mathbf{J}$ and equation (2.6) reduces to

$$\nabla \times \mathbf{H} = \mathbf{J} \tag{2.16}$$

Substituting equations (2.9) and (2.15) into (2.16)

$$\left(\nabla \times \frac{\mathbf{B}}{\mu}\right) = \mathbf{J_S} - \sigma \frac{\partial \mathbf{A}}{\partial t} \tag{2.17}$$

Using equation (2.12)

$$\left(\nabla \times \frac{1}{\mu}(\nabla \times \mathbf{A})\right) = \mathbf{J_S} - \sigma \frac{\partial \mathbf{A}}{\partial t} \tag{2.18}$$

Assuming a homogeneous medium and using the vector identity

$$\nabla \times (\nabla \times \mathbf{A}) = \nabla(\nabla \bullet \mathbf{A}) - \nabla^2 \mathbf{A} \tag{2.19}$$

we arrive

$$\frac{1}{\mu}\nabla^2 \mathbf{A} = \sigma \frac{\partial \mathbf{A}}{\partial t} - \mathbf{J_S} \tag{2.20}$$

where $\nabla \bullet \mathbf{A} = 0$ choosing the Coulomb gauge.

Assuming that the fields vary harmonically in steady state we can express $\mathbf{A}$ as

$$\mathbf{A} = \mathbf{A_0} e^{-jwt} \tag{2.21}$$

where w is the angular frequency.

Substituting (2.21) into (2.20), we obtain

$$\frac{1}{\mu}\nabla^2 \mathbf{A} = jw\sigma \mathbf{A} - \mathbf{J_S} \tag{2.22}$$

The solution of equation (2.22) can be obtained analytically only for very simple geometries such as infinite half plane media.

2.3. Skin Effect

Eddy currents are closed loops of induced currents circulating in planes perpendicular to the magnetic flux. They are oriented parallel to the coil winding and are limited to the area of the inducing magnetic field. Excitation frequency determines the depth of penetration into the specimen; as frequency increased, the depth of penetration decreases and the eddy current distribution becomes denser near the specimen's surface. This is known as the skin effect. This implies that test frequency also affects the sensitivity to changes in material properties and defects.

The depth of penetration depends on the operating frequency and properties of material such as electrical conductivity and magnetic permeability. The value of the skin depth can be determined from Maxwell's equation as follows [13].

Using equation (2.11), equation (2.16) can be written as

$$\nabla \times \mathbf{H} = \sigma \mathbf{E} \tag{2.23}$$

Taking the curl on both sides

$$\nabla \times (\nabla \times \mathbf{H}) = \nabla \times (\sigma \mathbf{E}) \tag{2.24}$$

Using the vector identities in equation (2.19), equation (2.24) can be written as

$$-\nabla^2 \mathbf{H} + \nabla \times (\nabla \bullet \mathbf{H}) = \nabla \times (\sigma \mathbf{E}) \tag{2.25}$$

From equation (2.7), $\nabla \bullet \mathbf{H} = 0$ and hence equation (2.25) reduces to

$$\nabla^2 \mathbf{H} = -\nabla \times (\sigma \mathbf{E}) \tag{2.26}$$

From equation (2.5) and (2.9), we have

$$\nabla \times \mathbf{E} = -\frac{\partial \mathbf{B}}{\partial t} = -\mu \frac{\partial \mathbf{H}}{\partial t} \tag{2.27}$$

Substituting equation (2.27) into equation (2.26)

$$\nabla^2 \mathbf{H} = \mu\sigma \frac{\partial \mathbf{H}}{\partial t} \tag{2.28}$$

Assuming the field varies harmonically in the steady state with time $\mathbf{H}$ can be expressed as

$$\mathbf{H} = \mathbf{H}_0 e^{jwt} \tag{2.29}$$

where w is the angular frequency.

Substituting equation (2.29) into (2.28), we have

$$\begin{aligned} \nabla^2 \mathbf{H} &= (jw\mu\sigma)\mathbf{H} \\ &= \mathrm{k}^2 \mathbf{H} \end{aligned} \tag{2.30}$$

where $\mathrm{k}^2 = jw\mu\sigma$.

For an infinite sheet of current in the $\mathbf{Y}$ direction on the $\mathbf{YZ}$ plane the magnetic field intensity is in the $\mathbf{Z}$ direction with no components in $\mathbf{X}$ or $\mathbf{Y}$ directions. Hence, equation (2.30) reduces to

$$\frac{\partial^2 \mathbf{H_z}}{\partial \mathrm{x}^2} = \mathrm{k}^2 \mathbf{H_z} \tag{2.31}$$

And the solution to equation (2.31) is given by

$$\mathbf{H_z} = \mathbf{H_0} e^{-\mathrm{kx}} \tag{2.32}$$

where k is defined by equation (2.30), called the propagation constant, is given by

$$\begin{aligned} \mathrm{k} &= (\mathrm{jw}\mu\sigma)^{1/2} \\ &= \left(\frac{w\mu\sigma}{2}\right)^{1/2} + j\left(\frac{w\mu\sigma}{2}\right)^{1/2} \end{aligned} \tag{2.33}$$

Hence, equation (2.32) can be written as

$$\mathbf{H_z} = \mathbf{H_0} e^{-\mathrm{x}/\delta} e^{-\mathrm{jx}/\delta} \tag{2.34}$$

where $\delta = \frac{1}{\sqrt{\pi f \mu \sigma}}$ that is called as the skin depth.

The standard depth of penetration is defined as the depth at which eddy current density has decreased to 1/e or 36.8% of the surface value. The skin depth (δ) is often used as a guideline to select the excitation frequency for a given test specimen. It is computed as

$$\delta = \frac{1}{\sqrt{\pi f \mu \sigma}} \tag{2.35}$$

where f is excitation frequency, μ is magnetic permeability of material and σ is electrical conductivity of the target material. Although the induced fields and currents can reach deeper than one standard depth of penetration, the eddy current density decreases very rapidly. At the two standard depths of penetration (2δ), the eddy current density decreases to $(1/e)^2$ or 13.5% of the surface density. At the three standard depths of penetration (3δ), it decreases to 5% of the surface density.

2.4. Multi-Frequency Eddy Current Testing

Multi-Frequency eddy current testing is usually used in non-destructive evaluation where the defect signal is distorted, due to superposition of contribution from other structures in the test geometry. Artifacts, such as specimen geometric boundaries or attached conductive objects, generate their own impedance plane trajectories during eddy current testing. A major problem in the analysis of SG tube inspection is the corruption of defect signal by a large contribution from tube support plate (TSP).

As an example, consider the tube and support plate shown in Figure 2.3. This configuration is typical of coolant tubes found in pressurized steam generators, such as

those used in nuclear power plants. The tube projects through support plates arranged within the steam generator [15]. Eddy current testing of these tubes is conducted to determine their structural condition. Specifically, the tubes are examined for corrosion pitting, dents and build-up of sludge [16].

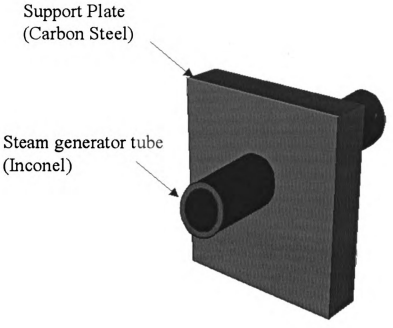

Figure 2.3 Steam generator tube with support plate

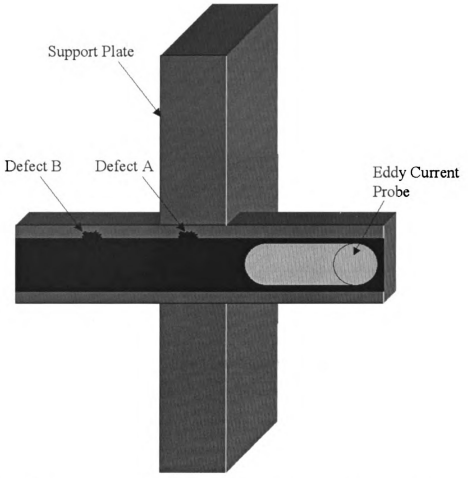

Figure 2.4 Cutaway View of steam generator tube with support plate and defects

The problem of distortion of defect signals in single-frequency eddy current testing is illustrated in Figure 2.4 that shows a cut-away view of Figure 2.3. There are two defects, A and B, in the tube. As the Eddy current probe passes through the tube, the impedance plane trajectory of defect B will be visible because there is no structure in the vicinity. However, the trajectory generated by defect A will be distorted, since the support plate is a conducting material and will also generate an eddy current signal trajectory as the probe passes it. The superposition of the support plate's signal with that of defect A makes the resulting trajectory more complicated. This distortion makes defect detection difficult.

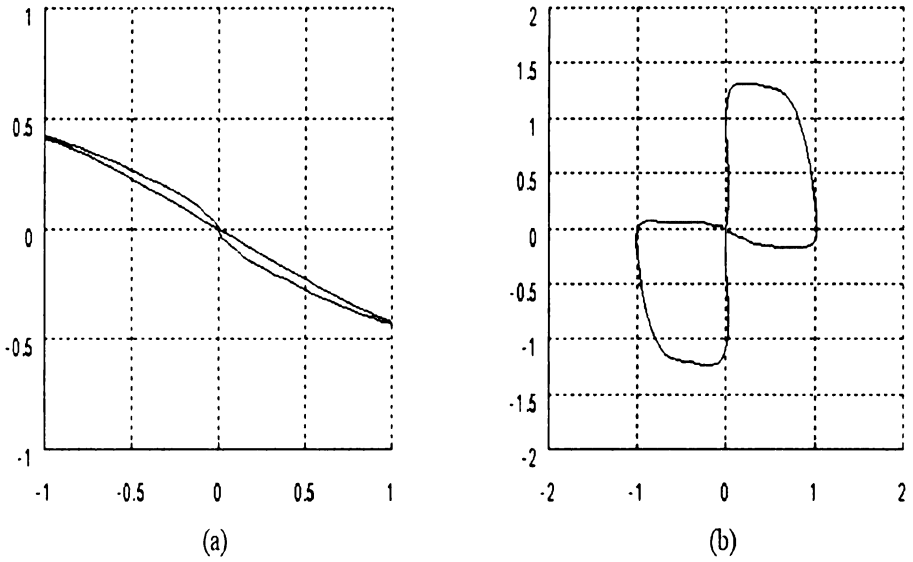

Figure 2.5 Simulated Eddy Current Impedance Plane Trajectories due to:
(a) defect (b) support plate

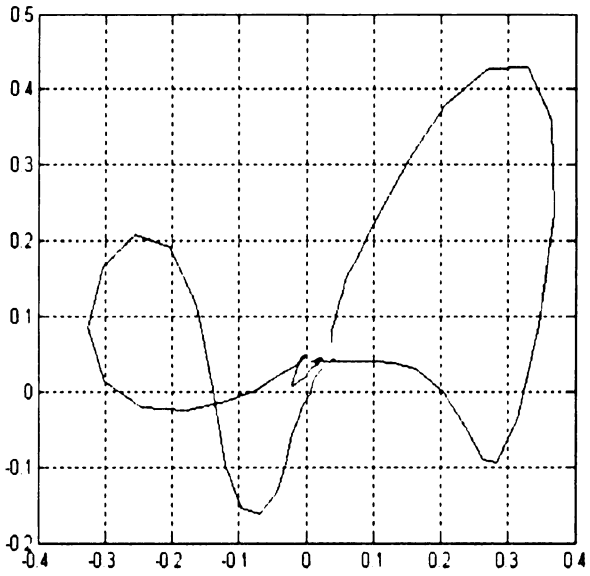

Figure 2.6 Impedance Plane Trajectories of a defect close to a support plate

Figure 2.5 shows simulated data representing eddy current trajectories generated by defect in tube and support plate and Figure 2.6 shows the impedance plane trajectory when the defect is in close proximity to the support plate. In addition to this distortion shown in Figure 2.6, the presence of noise also deteriorates the impedance plane trajectory of a defect, making data interpretation difficult. Filtering of the eddy current signal may eliminate much of the problems due to noise, but does not make the task of extracting defect information any easier due to the problem of superposition.

Multi-frequency Eddy current technique (MFECT) is commonly used for solving this problem. In MFECT, two or more sinusoidal signals of different frequencies are fed into a single eddy current probe and the gain and the phase signal from each frequency is collected separately. As it is shown in the previous section, the depth of penetration and phase lag are a function of test frequency; increasing test frequency reduces the depth of penetration and increases phase lag. Hence, it is possible to change the eddy current response by changing the test frequency and use this information to remove the unwanted signals.

2.5. Analysis of Multi-Frequency Eddy Current Testing (MFECT)

The aim of multi-frequency eddy current testing is to suppress artefacts affecting the defect impedance trajectory. This method of defect discrimination begins with identification of desired and undesired features. Desired features are typically defects and undesired features are artefacts that make eddy current characterization of defect difficult. When a high frequency is used as excitation frequency, inner diameter (ID) defect are more predominant in the signal. At intermediate frequency, all features in the wall are detectable and there is phase discrimination between internal and external defect signals. At low

frequency, there is a predominant signal from TSP with little phase separation between internal and external defect signals. In MFECT, signals are collected separately at a low and high frequencies. The high frequency ECT signal is rotated to match the low frequency ECT signal. The amplitude of high frequency ECT data is also scaled to match the low frequency ECT signal. On subtracting the transformed high frequency signal from the low frequency signal, the signal from TSP is largely reduced and only defect signal will remain as output signal. This process is also referred to as mixing.

Signal processing methods employed in analyzing MFECT data can be classified into three classes. Specifically, these are the algebraic, coordinate transform and phase rotation and subtraction method. All the methods assume that the signal contribution from the defect and the artefacts superpose linearly to form the eddy current impedance trajectory. This is often an erroneous assumption. Even though it is reasonable to assume linearity with respect to the excitation function at low excitation level, the system response is not linear with respect to the material property distribution in the domain of interest. Nevertheless, under some restrictive conditions, linearity may be assumed [17].

2.5.1. Algebraic Method

The algebraic method assumes that the multi-frequency data are linear function of n parameters. This assumption has been shown to be valid experimentally, under small signal conditions [18]. Furthermore, these parameters represent n inhomogeneities or attributes within the specimen [19]. To maintain the validity of this model, small signal conditions are assumed such that there is a linear relationship between variations in the parameters and the probe coil impedance. The complex impedance phasor of the test coil is represented by its

real (x-axis) and imaginary (y-axis) values. In case of two frequencies testing of four parameters, the coil impedance is expressed as

$$
\begin{aligned}
x_1 &= a_{11}P_1 + a_{12}P_2 + a_{13}P_3 + a_{14}P_4 \\
y_1 &= a_{21}P_1 + a_{22}P_2 + a_{23}P_3 + a_{24}P_4 \\
x_2 &= a_{31}P_1 + a_{32}P_2 + a_{33}P_3 + a_{34}P_4 \\
y_2 &= a_{41}P_1 + a_{42}P_2 + a_{43}P_3 + a_{44}P_4
\end{aligned}
$$

where (2.36)

x_1 : ohmic resistance at frequency1

y_1 :inductive reactance at frequency1

x_2 : ohmic resistance at frequency 2

y_2 :inductive reactance at frequency 2

P_i : Observed specimen parameters

a_{ij} :Coefficient of j^{th} parameter

In matrix notation, it is expressed as

$$\mathbf{AP} = \mathbf{C}$$

where (2.37)

$$\mathbf{A} = \begin{bmatrix} a_{11} & a_{12} & a_{13} & a_{14} \\ a_{21} & a_{22} & a_{23} & a_{24} \\ a_{31} & a_{32} & a_{33} & a_{34} \\ a_{41} & a_{42} & a_{43} & a_{44} \end{bmatrix}, \quad \mathbf{P} = \begin{bmatrix} P_1 \\ P_2 \\ P_3 \\ P_4 \end{bmatrix} \text{ and } \mathbf{C} = \begin{bmatrix} x_1 \\ y_1 \\ x_2 \\ y_2 \end{bmatrix}$$

In this model the matrix **A** is unknown and only the elements of **C** are observed directly. Elements of **P** are measured prior to eddy current testing, during a calibration stage. Equation (2.37) shows the modulation of the parameter vector **P** by a modulation matrix **A**, generating a signal vector **C**. The modulation equation is assumed to represent the interaction between the system current flow within the test coil and the specimen characteristics [18].

The matrix **A** is determined in the calibration stage using calibration standards with

known elements of $\mathbf{P}$, and observing the elements of $\mathbf{C}$. Once the matrix $\mathbf{A}$ has been determined, it is applied to the signal vector $\mathbf{C}$ during eddy current testing of a specimen. The goal of the multiparameter method is to detect and isolate the actual parameters by separating or decoupling the system of equations represented by equation (2.37). A complete solution has the form

$$\mathbf{P} = \mathbf{A}^{-1}\mathbf{C} \tag{2.38}$$

The signal vector elements represent the in-phase (x) and quadrature (y) of eddy current data collected at different frequencies. Specifically, for the case of two frequencies testing, x_1 and y_1 are equivalent to the in-phase and quadrature coil impedance components at frequency 1, respectively. In the case of four parameters, a similar relationship holds for elements x_2 and y_2 at frequency 2.

Since decoupling the system of equations represented by equation (2.37) is of primary interest, a complete solution to equation (2.37) is not necessary. The decoupling of the elements of $\mathbf{P}$ is accomplished by the adjoint of matrix $\mathbf{A}$, contained within the inverse matrix $\mathbf{A}^{-1}$ [21]. It reduces equation (2.38) to

$$\mathbf{P} = \mathrm{adj}\left[\mathbf{A}^{-1}\right]\mathbf{C} \tag{2.39}$$

Therefore,

$$
\begin{aligned}
P_1 &= b_{11}x_1 + b_{12}y_1 + b_{13}x_2 + b_{14}y_2 \\
P_2 &= b_{21}x_1 + b_{22}y_1 + b_{23}x_2 + b_{24}y_2 \\
P_3 &= b_{31}x_1 + b_{32}y_1 + b_{33}x_2 + b_{34}y_2 \\
P_4 &= b_{41}x_1 + b_{42}y_1 + b_{43}x_2 + b_{44}y_2
\end{aligned}
\qquad (2.40)
$$

where

x_1, y_1 : frequency 1 data elemenets of **C**

x_2, y_2 : frequency 2 data elements of **C**

P_i : Observed specimen parameters

b_{ij} : Coefficient of j^{th} parameter of adj[**A**]

The coefficients b_{ij} are determined using equation (2.39), or by using iterative numerical methods [19].

2.5.2. Phase Rotation and Subtraction Method

The objective of the phasor rotation and subtraction method is to discriminate the defect by subtracting out the effect of the artifacts. For suppression of unwanted artefact, an auxiliary frequency is utilized. This frequency is selected such that the eddy current probe is particularly sensitive to the presence of the undesired artefact. Due to the skin effect, low excitation frequencies are used to obtain signals that are sensitive to support plate and high excitation frequencies are used to obtain signals that are sensitive to probe wobble.

The subtraction of these undesired effects occurs in the mixing stage, after detection of the phase and magnitude of the probe coil signal. At this stage of signal processing, the eddy current data is resolved to the in-phase and quadrature components of the impedance plane. By transforming the auxiliary frequency trajectory to resemble its primary frequency trajectory, the data required for subtraction from the defect signal is obtained. The transformation of the auxiliary frequency artifact trajectory is accomplished through rotation,

translation and scaling. This procedure is typically executed manually, where an NDE analyst observes the stored complex impedance plane primary and auxiliary frequency trajectories due to the tube support plate.

The input data, x_a and y_a are applied to the scaling stage, which applies the transformation parameters S_x and S_y. The output of this step is applied to θ rotation combined with the translation parameters T_x and T_y. Then, the process is complete when the transformed auxiliary artifact signal is subtracted in the mixing stage from the distorted primary frequency defect trajectory. The output of typical two-parameter transformation is

$$x_r = x_p - \left[\left(S_x x_a \cos\theta + S_y y_a \sin\theta\right) - T_x\right]$$
$$y_r = y_p - \left[\left(-S_x x_a \sin\theta + S_y y_a \cos\theta\right) - T_y\right]$$

where
x_p, y_p : Input primary frequency data ordered pair
x_a, y_a : Input auxiliary frequency data ordered pair
x_r, y_r : Mixed output data ordered pair
S_x, S_y: Scaling parameters
T_x, T_y : Translation parameters
θ: Rotation parameter, degrees

(2.41)

Least Square Estimation

With properly chosen transformation parameters in equation (2.41), the effect of the artifact is minimized and the defect signal is more clearly defined. The optimal affine transform matrix parameters are estimated using a least squares estimation scheme [22]. By defining $\overline{C}_p$ as the primary frequency signal vector and $\overline{C}_a$ as the auxiliary frequency signal vector, the transformed $\overline{C}_a$ is expressed as

$$\overline{C}_a' = \overline{C}_a \cdot A\left(S_x, S_y, T_x, T_y, \theta\right) \tag{2.42}$$

The cost function E_{ls} is expressed as

$$\begin{aligned} E_{ls} &= \left\| \overline{C}_a' - \overline{C}_p \right\|^2 \\ &= \left\| \overline{C}_a A - \overline{C}_p \right\|^2 \end{aligned} \tag{2.43}$$

where $\|\cdot\|^2$ is the Euclidean norm.

The optimal values of the affine transform parameters are estimated by minimizing the cost function. This involves the solution of a simultaneous system of five equations

$$\frac{\partial E_{ls}}{\partial S_x} = 0 \tag{2.44}$$

$$\frac{\partial E_{ls}}{\partial S_y} = 0 \tag{2.45}$$

$$\frac{\partial E_{ls}}{\partial T_y} = 0 \tag{2.46}$$

$$\frac{\partial E_{ls}}{\partial T_y} = 0 \tag{2.47}$$

$$\frac{\partial E_{ls}}{\partial \theta} = 0 \tag{2.48}$$

Solutions of these equations yield the optimal affine transformation parameters. One of the iterative approaches to minimizing the cost function is the method of steepest descent. By choosing initial values for all five affine matrix parameters, the values are stepped iteratively so as to minimize the cost function. At each step, the gradient of the cost function is evaluated at the current parameter values.

Radial Basis Function Method

In mixing, a signal at a low excitation frequency is transformed to the corresponding signal at high frequency and the transformed signal is subtracted from the measured high frequency signal [4, 22]. In this approach, a radial basis function (RBF) neural network is applied to obtain transformation parameters. The architecture of RBF neural network is shown in Figure 2.7.

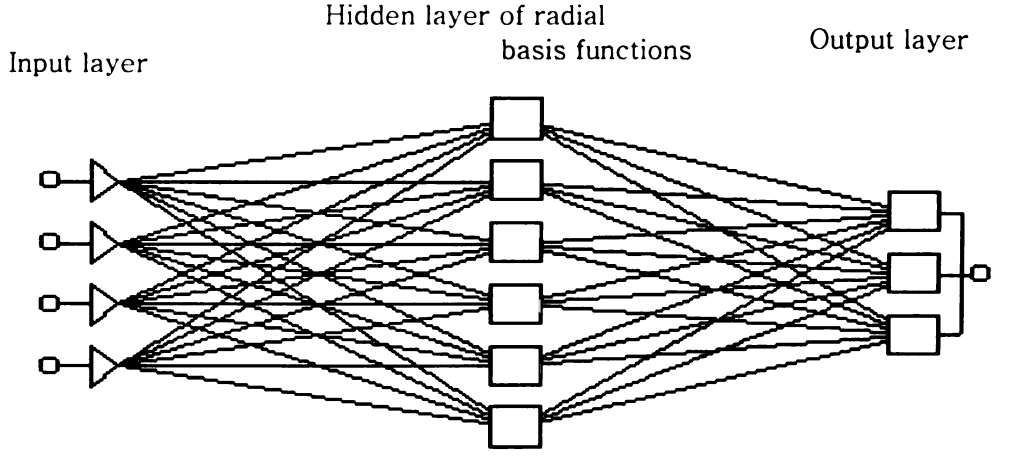

Figure 2.7 Architecture of RBF neural network

The RBF network output is a function F that has the following form.

$$F(x_i) = \sum_{i=1}^{N} w_i \varphi(\|x - x_i\|) \tag{2.49}$$

where x_i is the input at the ith input node, $\varphi(\bullet)$ is a set of arbitrary functions known as the radial basis functions, $\|\bullet\|$ denotes Euclidean norm and w_i constitutes a set of linear weights. During calibration, the set of weights are computed using known signals at frequencies f_1 and f_2.

Using one of these methods described above, the signal at frequency f_1 is transformed to the corresponding signal at frequency f_2. The residual is obtained by subtracting

transformed signal from the signal at frequency f_2 that contains only the defect signal with the contribution from artifacts suppressed to a large degree.

However, such approaches have significant errors when the data is not similar to data used to generate the mixing parameters. Consequently the parameters of mixing algorithm depend strongly on the data in the standard calibration file. When the parameters derived using calibration data is not optimal for a test signal the complementation of ICA results in a large residual which is difficult to interpret. In this thesis, an alternate approach to linear mixing algorithms based on the use of independent component analysis (ICA) is investigated to separate out signals due to defects and external support plates from noise. ICA is a method that depends on only the observed signal. In this thesis it is has also been used for noise filtering. The theoretical basis of independent component analysis is discussed in the next chapter.

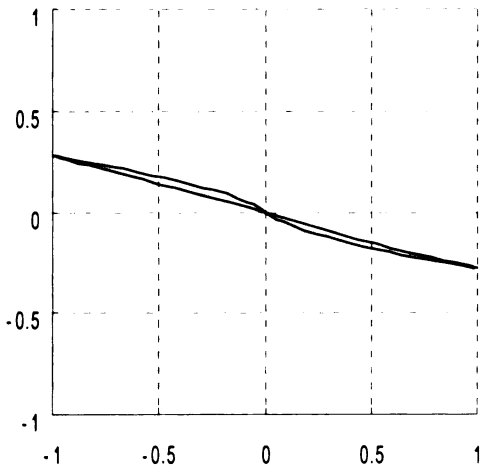
1
0.5
0
-0.5
-1
-1
-0.5
0
0.5
1

(a)

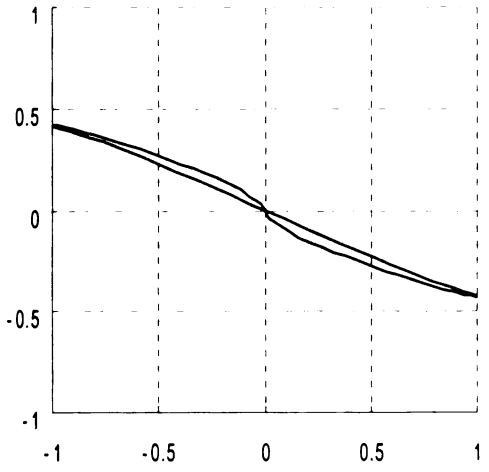
1
0.5
0
-0.5
-1
-1
-0.5
0
0.5
1

(b)

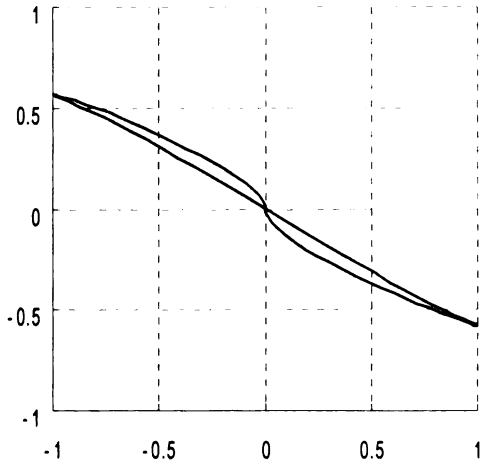
1
0.5
0
-0.5
-1
-1
-0.5
0
0.5
1

(c)

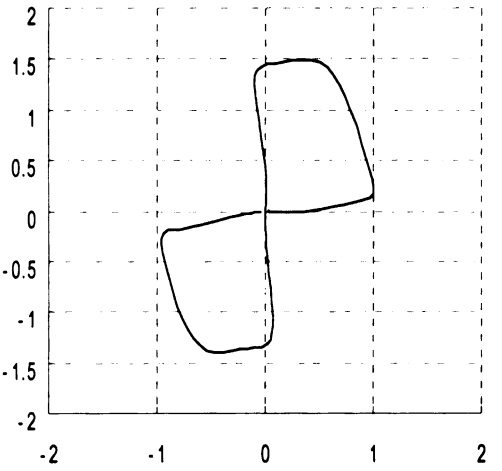
2
1.5
1
0.5
0
-0.5
-1
-1.5
-2
-2
-1
0
1
2

(f)

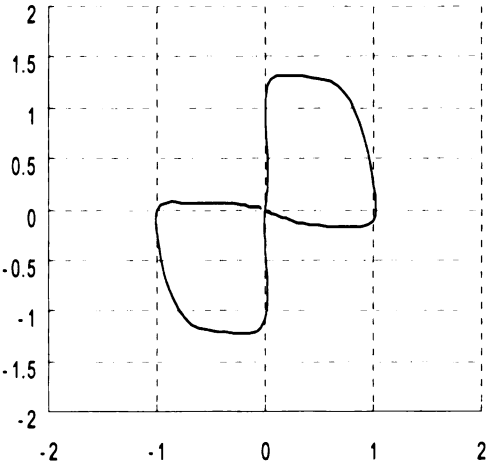
2
1.5
1
0.5
0
-0.5
-1
-1.5
-2
-2
-1
0
1
2

(g)

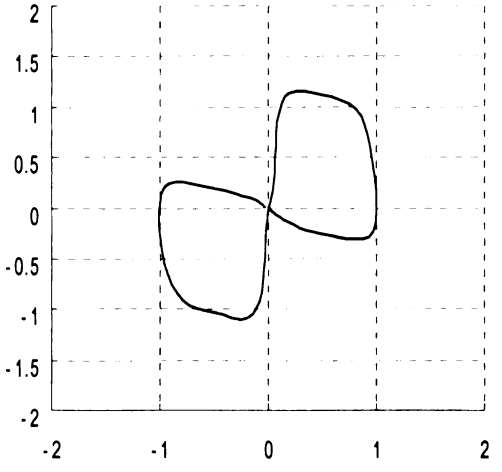
2
1.5
1
0.5
0
-0.5
-1
-1.5
-2
-2
-1
0
1
2

(h)

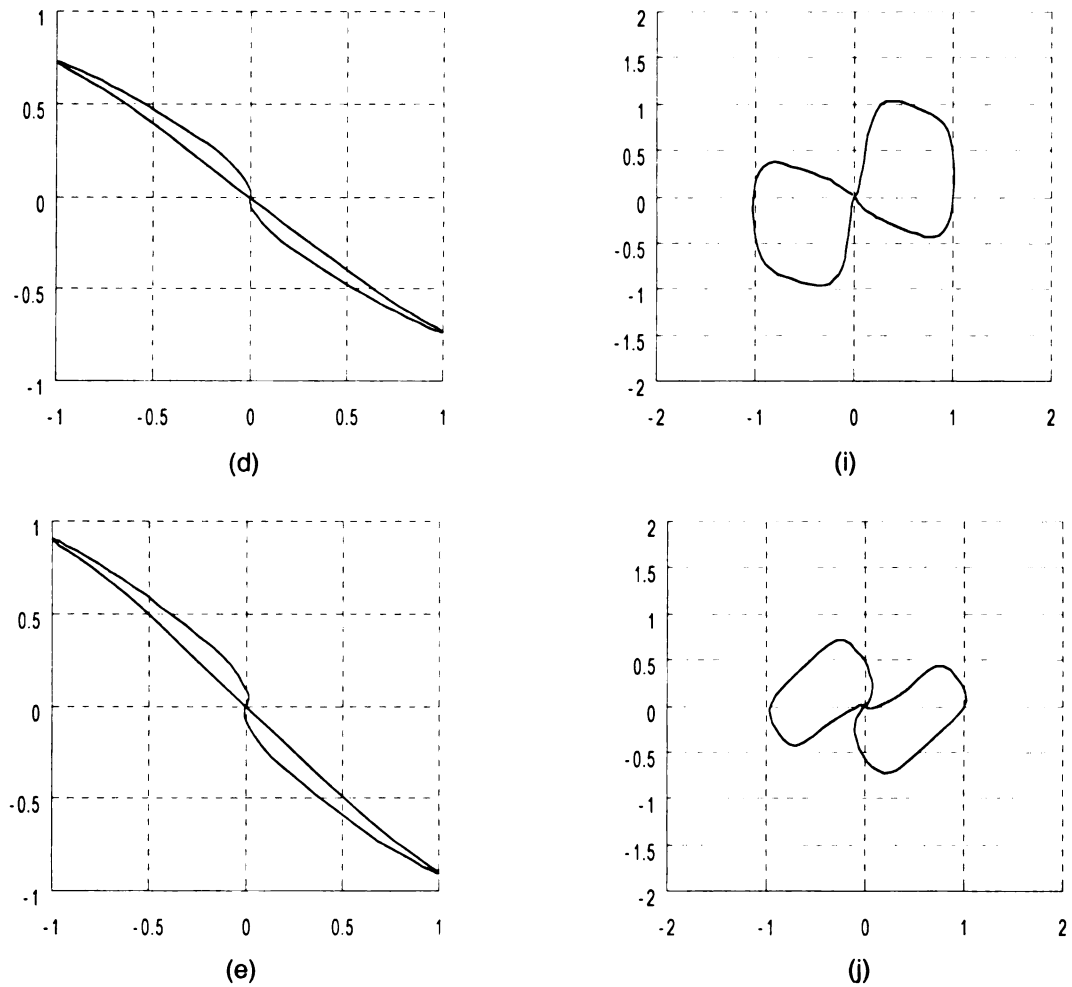

Figure 2.8 Normalized Simulated Impedance Plane Trajectories of Defect at excitation frequency: (a) 50 kHz, (b) 75 kHz, (c) 100 kHz, (d) 125 kHz, (e) 150 kHz, and Support Plate at excitation frequency (f) 50 kHz, (g) 75 kHz, (h) 100 kHz, (i) 125 kHz, (j) 150 kHz

3. INDEPENDENT COMPONENT ANALYSIS (ICA)

3.1. Principles of ICA

Independent Component Analysis (ICA) is a statistical method for extracting the source signals from a set of observed signals that can be expressed as mixtures of multiple sources. This problem is analogous to the human ability to distinguish a certain sound in the presence of different kinds of sounds. For instance, a human being can distinguish the sound of a violin from the recording of music by an orchestra. Hence, it can be said that ICA attempts to mimic this ability.

The data from a set of two source signals s_1 and s_2 can be represented by a set of simple linear equations.

$$\begin{aligned} x_1 &= a_{11}s_1 + a_{12}s_2 \\ x_2 &= a_{21}s_1 + a_{22}s_2 \end{aligned} \tag{3.1}$$

where a_{11}, a_{12}, a_{21} and a_{22} are mixing parameters that depend on the experimental conditions, x_1 and x_2 are the measured signals from a mixture of 2 source signals, s_1 and s_2.

When the coefficients a_{11}, a_{12}, a_{21} and a_{22} are known, it is straightforward to find the source signals from the above equations using classical inversion methods. In real world problems, however, these coefficients are seldom known which makes the solution of these equations very complex. The Independent Component Analysis method based on the central limit theorem provides a technique for achieving this goal [23]. The central limit theorem states that, as the number of independent, identically distributed random variables increases, the cumulative density function (CDF) of the sum will approach the CDF of a Gaussian

random variable. It is assumed that the source signals are independent and identically distributed in the rest of this thesis. Hence, measuring the gaussianity of a signal and minimizing the gaussianity provides a way of finding individual components. A major issue with this approach is selection of a metric that measures the gaussianity of a signal. The details of the method for measuring gaussianity will be discussed in this chapter.

The general statistical model is defined below. Suppose that there are n linear mixtures and n independent sources. Each of the mixtures is assumed to be a linear weighted sum of the original signals from n sources.

$$\begin{aligned} x_1 &= a_{11}s_1 + a_{12}s_2 + \cdots + a_{1n}s_n \\ x_2 &= a_{21}s_1 + a_{22}s_2 + \cdots + a_{2n}s_n \\ &\cdots \\ x_j &= a_{j1}s_1 + a_{j2}s_2 + \cdots + a_{jn}s_n \\ &\cdots \\ x_n &= a_{n1}s_1 + a_{n2}s_2 + \cdots + a_{nn}s_n \end{aligned} \tag{3.2}$$

The time index, t is omitted because $\mathbf{x}$ and $\mathbf{s}$ are regarded as random variables and $x(t)$ is obtained as samples of the random variable. The observed signal $\mathbf{x}$ and original signal $\mathbf{s}$ are assumed to have zero mean without loss of generality. Otherwise, a pre-processing step can be applied to subtract the sample mean to make them zero-mean random variables.

The equations (3.2) can be represented in matrix form as

$$\mathbf{x} = \mathbf{A}\mathbf{s} \tag{3.3}$$

where $\mathbf{x} = [x_1 \quad x_2 \quad \ldots \quad x_n]^T$ and $\mathbf{s} = [s_1 \quad s_2 \quad \ldots \quad s_n]^T$.

The above ICA model is a generative model, which means that the observed data are generated by a process of mixing the components $\mathbf{s}$ using the mixing matrix $\mathbf{A}$ which is

unknown. The aim of independent component analysis is to estimate the unmixing matrix $\mathbf{W}$ using statistical principles and computations. Eventually, the original source signals can be found as

$$\hat{\mathbf{s}} = \mathbf{W}\mathbf{x} \tag{3.4}$$

where $\hat{\mathbf{s}}$ is the estimated source signal.

The ICA method estimates the source signals up to a constant. This is because both the mixing matrix and original signals are unknown and any scalar multiplier can be cancelled by dividing the corresponding column by the scalar. The sign of the signal is ambiguous for the same reason. Another characteristic of ICA is that the order or position of the original signal cannot be determined. The order of source signals can be changed freely during the process and any component can be the first source because both the mixing matrix and original signals are unknown. Figure 3.1 shows the schematic overview of the ICA algorithm. The input data collected consists of a number of recordings which is larger than the number of expected source signals. The next two steps consist of preprocessing and ICA algorithm which are investigated at chapter 3.2 and 3.3, respectively. At the output stage, we obtain the estimated source signals using the unmixing matrix found using the ICA algorithm.

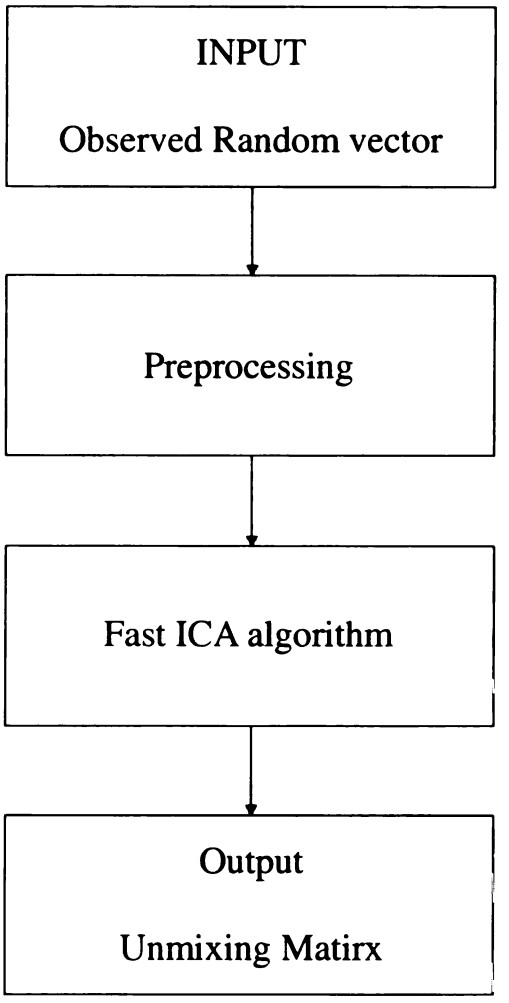

Figure 3.1 Schematic overview of ICA Process

3.2. Preprocessing

A preprocessing stage is required before applying ICA for better conditioning of the input data. Generally it consists of centering and whitening the data. Centering is the simple process of subtracting mean value from original data to obtain a zero mean signal. After estimating the original signals, it is necessary to add the subtracted mean value to the estimated signals. The second step is whitening of the observed variables. The purpose of whitening is to obtain a new vector in which the components are uncorrelated and variance of each signal is unity. The most popular method for whitening is using eigenvalue decomposition (EVD) of covariance matrix $E\{\mathbf{x}\mathbf{x}^T\} = \mathbf{E}\mathbf{D}\mathbf{E}^T$ where $\mathbf{E}$ is the orthogonal matrix of eigenvectors of $E\{\mathbf{x}\mathbf{x}^T\}$ and $\mathbf{D}$ is the diagonal matrix of eigenvalues of $E\{\mathbf{x}\mathbf{x}^T\}$ [24]. The whitening transform is implemented as

$$\mathbf{x}' = \mathbf{E}\mathbf{D}^{-1/2}\mathbf{E}^T\mathbf{x} \tag{3.5}$$

Using the whitening process, the orthogonal mixing matrix $\mathbf{A}'$ can be computed as

$$\begin{aligned} \mathbf{x}' &= \mathbf{E}\mathbf{D}^{-1/2}\mathbf{E}^T\mathbf{x} = \mathbf{E}\mathbf{D}^{-1/2}\mathbf{E}^T\mathbf{A}\mathbf{s} = \mathbf{A}'\mathbf{s} \\ \mathbf{A}' &= \mathbf{E}\mathbf{D}^{-1/2}\mathbf{E}^T\mathbf{A} \end{aligned} \tag{3.6}$$

By using the above transform, the orthogonal mixing matrix $\mathbf{A}'$ is obtained. When the variance of independent component is assumed to be unity, it can be seen that

$$E\{\mathbf{x}'\mathbf{x}'^T\} = \mathbf{A}'E\{\mathbf{s}\mathbf{s}^T\}\mathbf{A}'^T = \mathbf{A}'\mathbf{A}'^T = \mathbf{I} \tag{3.7}$$

Because $\mathbf{A}'$ is orthogonal matrix, $\mathbf{A}'^T$ is equal to the inverse of $\mathbf{A}'$. Hence, the transformation reduces the number of parameters that need to be calculated to find the unmixing matrix. When the dimension of matrix is large, the whitening step reduces the

computational time and storage considerably. As a result of whitening, the measured data is also transformed to be uncorrelated and have a unit variance. In this thesis, it is assumed that centering and whitening is performed on the measured signals.

3.3. Independent Component Analysis Based on Gaussianity

The main concept of ICA is inspired by the central limit theorem which states that, as the number of independent, identically distributed (i.i.d.) random variables increases, the cumulative density function (CDF) of the sum approaches the CDF of Gaussian random variable. Under the assumption that the different source signals are independent to each other, the original signal can be reconstructed when minimum gaussianity of the random variable is observed. Let $x_1,x_2,\ldots,x_n$ be a sequence of i.i.d. variables and let s_n be the sum of n random variables.

$$s_n = x_1 + x_2 + \ldots + x_n \tag{3.8}$$

No matter what the distributions of random variables $x_1,x_2,\ldots,x_n$ are, the CDF of s_n approaches the Gaussian distribution as n increases. Therefore, if gaussianity is measured using some method, it will be a monotonically increasing function of the number of independent components. On the other hand, gaussianity will be minimized when s_n contains only one component. When minimum gaussianity is observed, the corresponding signal can be regarded as an estimate of one component of the original signals. Hence, it is very critical to find a metric to measure the gaussianity of random variables.

Measuring Gaussianity

The classical method for measuring gaussianity is based on using kurtosis, the fourth

order moment [25]. Kurtosis is widely used to measure gaussianity because of its computational simplicity. Another method, which uses negentropy, is based on information theory and differential entropy. These two methods are described next.

For a random variable $\hat{\mathbf{s}}$, kurtosis is defined as

$$Kurtosis(\hat{\mathbf{s}}) = E\{\hat{\mathbf{s}}^4\} - 3(E\{\hat{\mathbf{s}}^2\})^2 \tag{3.9}$$

where E is expectation operator.

Since $\hat{\mathbf{s}}$ is assumed to be zero-mean, unit-variance random variable, kurtosis is simplified as

$$Kurtosis(\hat{\mathbf{s}}) = E\{\hat{\mathbf{s}}^4\} - 3 \tag{3.10}$$

This is the normalized version of fourth moment of a random variable. For a Gaussian random variable, the fourth moment is equal to $3(E\{\hat{\mathbf{s}}\}^2)^2$. Therefore, kurtosis is zero for Gaussian random variable and is positive or negative for non–Gaussian variables. Positive kurtosis is referred to as supergaussian property for which the distribution is more similar to that of a Gaussian distribution. A spike at the middle and approaching zero at the tails characterize positive kurtosis. Negative kurtosis refers to subgaussian property and is characterized by a relatively flat distribution.

To illustrate how the original signal is reconstructed using kurtosis, we need to know the properties of kurtosis. When x_1 and x_2 are independent to each other, kurtosis has following properties.

$$\begin{aligned} Kurtosis(x_1 + x_2) &= Kurtosis(x_1) + Kurtosis(x_2) \\ Kurtosis(\alpha x_1) &= \alpha^4 Kurtosis(x_1) \end{aligned} \tag{3.11}$$

where α is a scalar.

Let us assume that $E\{(\mathbf{w}^T\mathbf{x})^2\}=1$ and let the two-dimensional mixing model be given by $\mathbf{x}=\mathbf{As}$ where random variable $\mathbf{x}$ is the measured data, $\mathbf{s}$ is the original source signals and $\mathbf{A}$ is a 2 by 2 mixing matrix. Define another vector $\mathbf{z}=\mathbf{A}^T\mathbf{w}$. It can be shown that

$$E\{(\mathbf{w}^T\mathbf{x})^2\}=E\{\mathbf{w}^T\mathbf{A}\mathbf{A}^T\mathbf{w}\}=\|\mathbf{z}\|^2=1 \quad \text{where} \quad E\{\mathbf{s}\mathbf{s}^T\}=\mathbf{I} \tag{3.12}$$

Under the constraint $\|\mathbf{z}\|^2=1$, kurtosis function has a number of local minima and maxima. To make the argument clearer, let us assume that one component has negative kurtosis and the other component has positive kurtosis.

Let $\hat{\mathbf{s}}$ be the weighted vector of $\mathbf{x}$.

$$\hat{\mathbf{s}}=\mathbf{w}^T\mathbf{x}=\mathbf{w}^T\mathbf{A}\mathbf{s}=\mathbf{z}^T\mathbf{s}=z_1s_1+z_2s_2 \tag{3.13}$$

From properties of kurtosis, we have

$$\begin{aligned} Kurtosis(\hat{\mathbf{s}}) &= Kurtosis(z_1s_1)+Kurtosis(z_2s_2) \\ &= z_1^4\,Kurtosis(s_1)+z_2^4\,Kurtosis(s_2) \end{aligned} \tag{3.14}$$

Since $\hat{\mathbf{s}}$ and $\mathbf{s}$ are assumed to have unit-variance as a result of whitening in the preprocessing stage, we have unit variance of $\hat{\mathbf{s}}$ and $\mathbf{s}$.

$$E\{\hat{\mathbf{s}}^2\}=z_1^2E\{s_1^2\}+z_2^2E\{s_2^2\}=z_1^2+z_2^2=1 \tag{3.15}$$

It is clear that (z_1,z_2) is located on the unit circle that satisfies above equation. Now, the problem is to find one of the maximum values of $\left|z_1^4\,Kurtosis(s_1)+z_2^4\,Kurtosis(s_2)\right|$ with a constraint of $z_1^2+z_2^2=1$. Due to the assumption that kurtosis of s_1 and s_2 have different sign, it can be easily shown that the maximum value occurs when one element is zero and the other is $+1$ or -1. Therefore, there are 4 maximum values of

$\left| z_1^4 Kurtosis(s_1) + z_2^4 Kurtosis(s_2) \right|$ with a constraint of $z_1^2 + z_2^2 = 1$.

In practice, the strongest direction of initial weighting vector is computed (increasing direction for positive kurtosis, decreasing direction for negative kurtosis) based on the available samples of $\mathbf{x}$. Then, the gradient method is applied to find a new weighting vector $\mathbf{w}$. Because of this computational simplicity, kurtosis has been widely used for estimating ICA model. However, the disadvantage in using kurtosis as a metric of measuring gaussianity is that the accuracy of the estimate of kurtosis depends on the availability of adequate data particularly in the tail of distribution. This implies that kurtosis is not a robust method for measuring gaussianity. To compensate for this weakness, an alternate technique based on negentropy is used and is described next.

Negentropy is an alternate method to measure gaussianity of random variables that is based on information theory and provides a quantitative measurement of differential entropy. Entropy is an essential concept of information theory and it measures the amount of information contained in an observation. Entropy increases as the random variable becomes more unpredictable and unstructured [26].

Entropy, H, of a discrete random variable is defined as

$$H(\hat{\mathbf{s}}_{discrete}) = -\sum_i P(\hat{\mathbf{s}}_{discrete} = k_i) \log P(\hat{\mathbf{s}}_{discrete} = k_i) \tag{3.16}$$

where $\hat{\mathbf{s}}_{discrete}$ is a discrete random variable and k_i is a possible value of $\hat{\mathbf{s}}_{discrete}$ with probability density function (PDF), $P(\hat{\mathbf{s}}_{discrete})$.

For a continuous random variable, it is defined as

$$H(\hat{\mathbf{s}}_{continuous}) = -\int f(\hat{\mathbf{s}}_{continuous}) \log f(\hat{\mathbf{s}}_{continuous}) d\hat{\mathbf{s}}_{continuous} \tag{3.17}$$

where $\hat{\mathbf{s}}_{continuous}$ is the continuous random variable with PDF $f(\hat{\mathbf{s}}_{continuous})$.

From the fundamental proposition of information theory, a Gaussian random variable has larger entropy than any other random variable with the same variance. This implies that entropy can be used as a quantitative measure of gaussianity. To obtain a measure of gaussianity, the modified definition of differential entropy is used. It is called as negentropy and is defined as

$$J(\hat{\mathbf{s}}) = H(\hat{\mathbf{s}}_{Gauss}) - H(\hat{\mathbf{s}}) \tag{3.18}$$

where $\hat{\mathbf{s}}_{Gauss}$ is a Gaussian random variable which has the same covariance matrix with $\hat{\mathbf{s}}$.

By definition, negentropy is always positive and zero if and only if $\hat{\mathbf{s}}$ is Gaussian random variable. When the statistical property is considered, negentropy is a well-defined metric to measure non-gaussianity [26]. However, in general, negentropy has the disadvantage that it is very difficult to compute. Therefore, a modified approximation of negentropy that combines the strengths of kurtosis and negentropy is often used to measure the gaussianity.

A commonly used approximation of negentropy is given by

$$J(\hat{\mathbf{s}}) \approx \frac{1}{12} E\{\hat{\mathbf{s}}^3\}^2 + \frac{1}{48} \text{Kurtosis}(\hat{\mathbf{s}})^2 \tag{3.19}$$

where $\hat{\mathbf{s}}$ is zero mean, unit variance random variable. The above approximation includes the kurtosis function, which leads to issues of robustness of the metric. Also, it has been argued that cumulant-based approximations of negentropy are inaccurate in many cases [27,28]. Therefore, a new approximation method based on maximum-entropy principles is often used and is expressed as

$$J(\hat{\mathbf{s}}) \approx \sum_i k_i \left[E\{G_i(\hat{\mathbf{s}})\} - E\{G_i(\hat{\mathbf{s}}_{Gauss})\}\right]^2 \tag{3.20}$$

where k_i is a positive constant and $\hat{s}_{Gauss}$ is a standardized Gaussian random variable with zero-mean, the same variance as $\mathbf{s}$ and $G_i(s)$ is a function that does not grow faster than quadratically as a function of $|s|$ [28]. According to equation (3.20), negentropy is always positive and zero when $\hat{\mathbf{s}}$ is Gaussian. The choice of function G_i is very important. In the practical choice of the functions $G_i(s)$, the following criteria must be emphasized: First, $E\{G_i(s)\}$ should be estimated without statistical difficulty. Second, the maximum entropy method assumes that the density function $f(s)$ is integrable, because the expectation is obtained as

$$E\{G_i(s)\} = -\int f(s)G_i(s)ds \tag{3.21}$$

Therefore, G_i must not grow faster than quadratic function, because a function growing faster might lead to non-integrability [28]. Usually the following choices show robust and reliable results and are called contrast functions [10, 11].

$$G_1(u) = \frac{1}{a_1}\log\cosh(a_1 u) \qquad \text{(where } 1 \le a_1 \le 2\text{)} \tag{3.22}$$

$$G_2(u) = -e^{-\frac{u^2}{2}}$$

Approximations with the above G function have combined the advantages of two metrics, kurtosis and negentropy, used to measure gaussianity. It contains all the statistical information and is much easier to compute than negentropy. A practical algorithm, which is based on this approximation, is developed and is known as the Fast-ICA algorithm.

Fast-ICA Algorithm

Fast-ICA algorithm is one of the most powerful algorithms for estimating individual non-gaussian components in a mixture of source signals. The procedure of Fast-ICA

algorithm starts with choosing an initial weight vector $\mathbf{w}$, which is updated by the learning rule. With the chosen weight vector, gaussianity is measured by $J(\hat{\mathbf{s}})$ given in the equation (3.20). The purpose of Fast-ICA algorithm is to find a vector $\mathbf{w}$ such that its projection on $\mathbf{x}$, $\hat{\mathbf{s}} = \mathbf{w}^T\mathbf{x}$, minimizes gaussianity. There is a constraint that the variance of $\mathbf{w}^T\mathbf{x}$ is unity. When $\mathbf{x}$ is preprocessed, the norm of weight vector can be calculated from this constraint. Recall that the norm of preprocessed data is unity.

$$\left\|\mathbf{w}^T\mathbf{x}\right\|^2 = \mathbf{w}^T\mathbf{x}\mathbf{x}^T\mathbf{w} = \mathbf{w}^T\mathbf{w} = 1 \tag{3.23}$$

The Fast-ICA algorithm is based on a fixed points iteration scheme for finding a weight vector that minimizes the gaussianity of $\mathbf{w}^T\mathbf{x}$. The algorithm is derived from derivatives of the non-quadratic function G in (3.21). If the two functions in (3.21) are chosen, the derivatives are given by

$$\begin{aligned} &\frac{\partial G_1(u)}{\partial u} = g_1(u) = \tanh(a_1 u) \\ &\frac{\partial G_2(u)}{\partial u} = g_2(u) = u e^{-\frac{u^2}{2}} \end{aligned} \qquad (\text{where } 1 \le a_1 \le 2) \tag{3.24}$$

The details of Fast-ICA algorithm is summarized as follows:

1. Preprocessing: The data is first preprocessed with centering and whitening. Centering subtracts the mean to obtain a zero-mean signal and whitening produces components that are uncorrelated with unit variance, giving $\left\|\hat{\mathbf{s}}\right\| = \left\|\mathbf{w}^T\mathbf{x}\right\| = 1$ when $\left\|\mathbf{w}\right\| = 1$. Whitening also transforms the mixing matrix $\mathbf{A}$ to be orthogonal.
2. Select an initial, random weight vector $\mathbf{w}$ with the constraint $\left\|\mathbf{w}\right\| = 1$.

3. From (3.20), the negentropy is maximized when $E\{G(\hat{\mathbf{s}})\}$ is maximum or minimum since $E\{G(\hat{\mathbf{s}}_{Gauss})\}$ is a constant. Thus, the optimization process seeks to find optima of $E\{G(\hat{\mathbf{s}})\}$ under the constraint of $\|\hat{\mathbf{s}}\| = \|\mathbf{w}^T\mathbf{x}\| = 1$. It can be expressed as

$$F(\mathbf{w}) = E\{G(\mathbf{w}^T\mathbf{x})\} - \beta(\|\mathbf{w}\| - 1) \tag{3.25}$$

4. Using the Kuhn-Tucker theorem [29], the solution is obtained as a solution of following equation.

$$F'(\mathbf{w}) = E\{\mathbf{x}g(\mathbf{w}^T\mathbf{x})\} - \beta\mathbf{w}_i = 0 \tag{3.26}$$

where β is a constant called a Lagrange multiplier.

5. The updated weight vector $\mathbf{w}^+$ is obtained using Newton iteration [30] and is given by

$$\mathbf{w}^+ = E\{\mathbf{x}g(\mathbf{w}^T\mathbf{x})\} - E\{g'(\mathbf{w}^T\mathbf{x})\}\mathbf{w} \tag{3.27}$$

6. Normalize the updated vector

$$\mathbf{w}^{new} = \mathbf{w}^+ / \|\mathbf{w}^+\| \tag{3.28}$$

7. If $\mathbf{w}^{new} = \mathbf{w}^{old}$, $\hat{\mathbf{s}} = \mathbf{w}^T\mathbf{x}$ is an estimate of the source. Go to Step 2 to compute the next source signal. If not, go to Step 5.

When solving for multiple sources, $\mathbf{w}_i, i = 1,2,\ldots,n$ are obtained from the above process. The estimated sources $\mathbf{w}_1{}^T\mathbf{x}, \mathbf{w}_2{}^T\mathbf{x}, \ldots, \mathbf{w}_n{}^T\mathbf{x}$ are then uncorrelated after each component is obtained. Decorrelation is achieved by Gram-Schmidt decorrelation [31]. From this, the independent component is calculated one by one. When one obtains a new

weighting vector $\mathbf{w}_{p+1}^{\mathrm{T}}$, the projection $\mathbf{w}_{p+1}^{\mathrm{T}}\mathbf{w}_j, j = 1,2,\ldots,p$ on each of the previously estimated vectors is subtracted from $\mathbf{w}_{p+1}$, which is then normalized. Therefore, the separated independent components are unique up to a multiplicative sign and scale factor. The schematic overview of the process is illustrated in Figure 3.2.

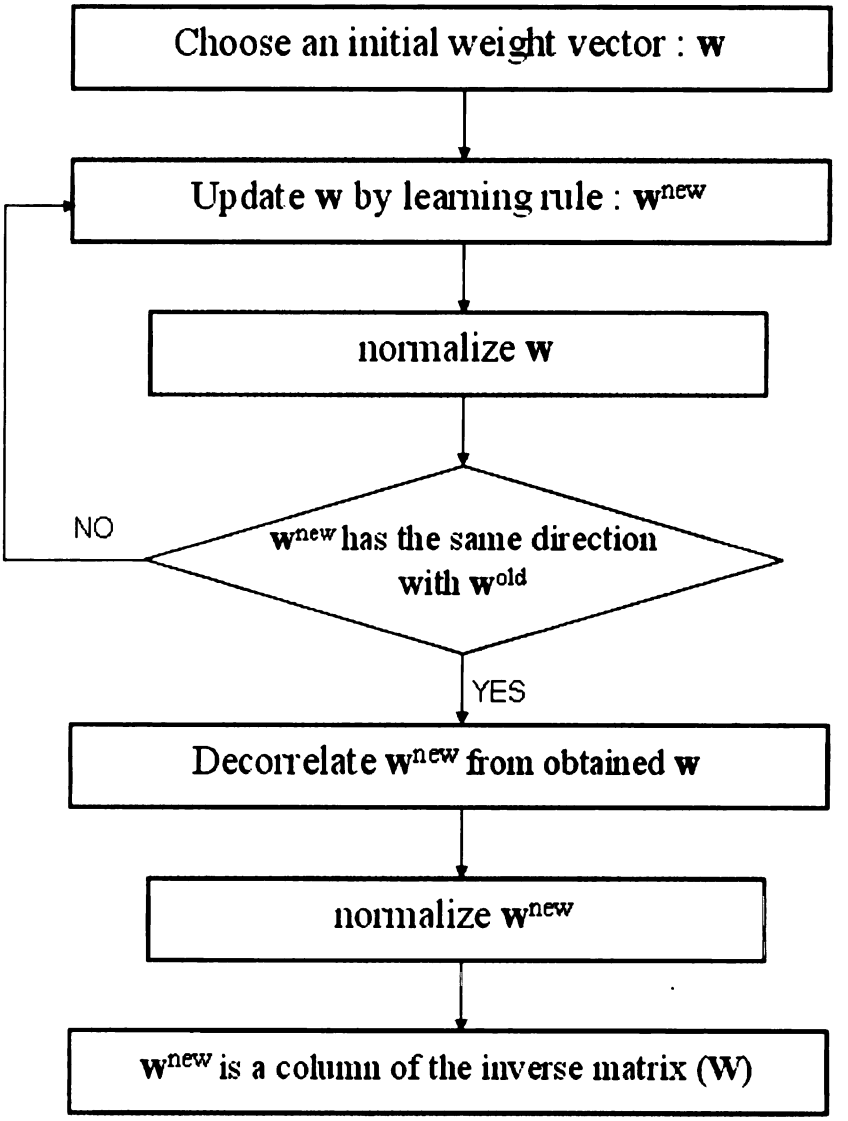

Figure 3.2 Flowchart of Fast–ICA Algorithm

Noisy ICA Model (Residue Theory)

The ICA model cab be used to extract source signals successfully when noise is usually present in the measurement. In general, methods taking noise explicitly into account assume that the noise has Gaussian distribution. As discussed before, the Fast ICA algorithm measures gaussianity of the mixture and minimizes it to extract a source signal. Therefore, Gaussian source signals cannot be extracted using independent component analysis.

However, when only one Gaussian noise signal is present in the mixture, ICA can find noise using residual theory. Residual theory states that a function $f(z)$ has a simple pole at z_0, we can write

$$f(z) = \frac{a_0}{z - z_0} + g(z) \tag{3.29}$$

where $g(z)$ is analytic at z_0, so that $(z - z_0)g(z) \to 0$ as $z \to z_0$. It follows that the residue is given by

$$a_0 = \lim_{z \to z_0} (z - z_0) f(z) \tag{3.30}$$

It is assumed that $f_j(z)$ is analytic in $\mathbf{C}$ except at z_j. For $j = 1,2,\cdots,k$, let $f_j(z)$ denote the principal part of $f(z)$ at z_j. Using this residue theory, Gaussian noise $g(z)$ can be found as

$$g(z) = f(z) - \sum_{j=1}^{k} f_j(z) \tag{3.31}$$

where $g(z)$ is analytic in $\mathbf{C}$, so that $\int_{\mathbf{C}} g(z) = 0$.

3.4. Independent Component Analysis Based on Mutual Information

Mutual information is another approach for ICA which measures the mutual dependence of the components of a transformed vector, $\mathbf{s}$ and then optimizes the unmixing matrix, $\mathbf{W}$ to minimize the measured dependence of each components. There are many methods to measure the mutual dependence and Shannon's mutual information is considered to be one of the popular choices.

Shannon`s mutual information between n random variables, $\hat{s}_i, i = 1,2,\cdots,n$, is defined as

$$I(\hat{\mathbf{s}}) = \sum_{i=1}^{n} H(\hat{s}_i) - H(\hat{\mathbf{s}}) \tag{3.32}$$

The mutual information, $I(\hat{\mathbf{s}})$, measures the amount of shared information in the components of $\hat{\mathbf{s}}$. It can also be considered as a measure of the independence of random variables. Naturally, it is also non-negative and is zero if and only if the components of $\hat{\mathbf{s}}$ are mutually independent with respect to each other. Hence, the primary purpose is to find a transform that minimizes the mutual information between measurements of original components [32]. One of the most important properties of mutual information is that it is invariant under continuous and monotonic transformations. Therefore, mutual information does not change unless the components are mixed. For invertible linear transformation $\hat{\mathbf{s}} = \mathbf{W}\mathbf{x}$, mutual information is defined as:

$$I(\hat{s}_1,\hat{s}_2,\ldots,\hat{s}_n) = \sum_i H(\hat{s}_i) - H(\mathbf{x}) - log|\det \mathbf{W}| \tag{3.33}$$

If $\hat{s}_i$ is uncorrelated and has unit variance, then the covariance matrix of $\hat{\mathbf{s}}$ is an identity matrix. Hence,

$$E\{\hat{\mathbf{s}}\hat{\mathbf{s}}^{\mathrm{T}}\} = \mathbf{W}E\{\mathbf{x}\mathbf{x}^{\mathrm{T}}\}\mathbf{W}^{\mathrm{T}} = \mathbf{I} \tag{3.34}$$

$$\det E\{\hat{\mathbf{s}}\hat{\mathbf{s}}^{\mathrm{T}}\} = \det \mathbf{W}E\{\mathbf{x}\mathbf{x}^{\mathrm{T}}\}\mathbf{W}^{\mathrm{T}} = \det \mathbf{W} \det E\{\mathbf{x}\mathbf{x}^{\mathrm{T}}\} \det \mathbf{W}^{\mathrm{T}} = \mathbf{I} \tag{3.35}$$

which implies that $\det \mathbf{W}$ always has a constant value. In this case, the equation (3.33) reduces to

$$I(\hat{s}_1, \hat{s}_2, \ldots, \hat{s}_n) = C - \sum_i J(\hat{s}_i) \tag{3.36}$$

From equation (3.36), we see that negentropy is in inverse proportion to mutual information. Mutual information and negentropy differs by a constant and sign difference for variables with unit variance. When the source signals are uncorrelated, minimizing mutual information of the estimated signals is equal to maximizing the gaussianity. Therefore, maximizing negentropy is equivalent to minimizing the mutual information of the separated components of $\hat{\mathbf{s}}$.

The use of mutual information is also motivated by the Kullback_Leibler divergence which is defined as:

$$\delta(f_1, f_2) = \int f_1(\hat{\mathbf{s}}) \log \frac{f_1(\hat{\mathbf{s}})}{f_2(\hat{\mathbf{s}})} d\hat{\mathbf{s}} \tag{3.37}$$

where f_1 and f_2 are probability density functions (PDF). The Kullback_Leibler divergence can be considered as a distance between two probability functions. If $\hat{s}_i$ in (3.32) are independent to each other, the joint probability function could be factorized as $f(\hat{s}_1 \hat{s}_2 \ldots \hat{s}_n) = f_1(\hat{s}_1) f_2(\hat{s}_2) \ldots f_n(\hat{s}_n)$. Thus, the independence of $\hat{s}_i$ can be measured by the Kullback-Leibler divergence between the real PDF and the factorized density function $\hat{f} = f_1(\hat{s}_1) f_2(\hat{s}_2) \ldots f_n(\hat{s}_n)$, where $f_i(\cdot)$ are the marginal density function of $\hat{s}_i$. Theoretically, the measured independence of $\hat{s}_i$ is equal to the mutual information of $\hat{s}_i$.

Kullback-Leibler divergence also shows that minimizing mutual information is closely related with maximizing likelihood. The likelihood is represented as a Kullback-Leibler distance between the observed density and a factorized density. The problem with mutual information is that the estimate of PDF is needed to obtain the entropy that restricts the use of mutual information in ICA implementation. This problem can be solved by using an approximation of mutual information based on polynomial density expansion [32], which is related to the Taylor expansion that gives an approximation of PDF. For example, if $\hat{\mathbf{s}}$ is a random variable having zero mean and unit variance, the first term of the Edgeworth expansion gives [33]:

$$f(\xi) \approx \varphi(\xi)\left[1 + k_3(\hat{s})h_3(\xi)/6 + k_4(\hat{s})h_4(\xi)/24 + \cdots\right] \tag{3.38}$$

where φ is the density function of a standardized Gaussian random variable, the $k_i(\hat{s})$ is the cumulants of $\hat{\mathbf{s}}$ (zero-mean, unit variance) and $h_i(\cdot)$ is a polynomial function. Using the above equations, the following approximation is obtained for mutual information.

$$I(\hat{\mathbf{s}}) \approx \mathbf{C} + \frac{1}{48}\sum_{i=1}^{m}\left[4k_3(\hat{s}_i)^2 + k_4(\hat{s}_i)^2 + 7k_4(\hat{s}_i)^4 - 6k_3(\hat{s}_i)^2 k_4(\hat{s}_i)\right] \tag{3.39}$$

where $\mathbf{C}$ is constant and $\hat{s}_i$ are uncorrelated to each other.

4. APPLICATION OF ICA TO NDT

4.1. Feature extraction algorithm

Multi-frequency eddy current testing (MFECT) is one of the most widely used methods for inspecting steam generator (SG) tubes in nuclear power plant. However, signal processing is often required to extract the relevant information from measurements because there are many factors including noise that affect the eddy current measurement. This thesis addresses the problem of separating the defect signal that is distorted by contributions from benign sources such as tube support plate (TSP) in steam generator inspection. Novel signal processing techniques have been proposed for mitigating difficulties encountered in solving the underlying inverse problem. Feature extraction techniques for eddy current signals are used to identify and eliminate irrelevant parts of the data generated by edge effects, probe lift-off noise and white noise. It is possible to look at the noise as derived signal from an additional source and develop a method, whose rationale is to separate the desired signal from the other interfering signals. Figure 4.1 shows the basic scheme of using ICA to MFECT data analysis.

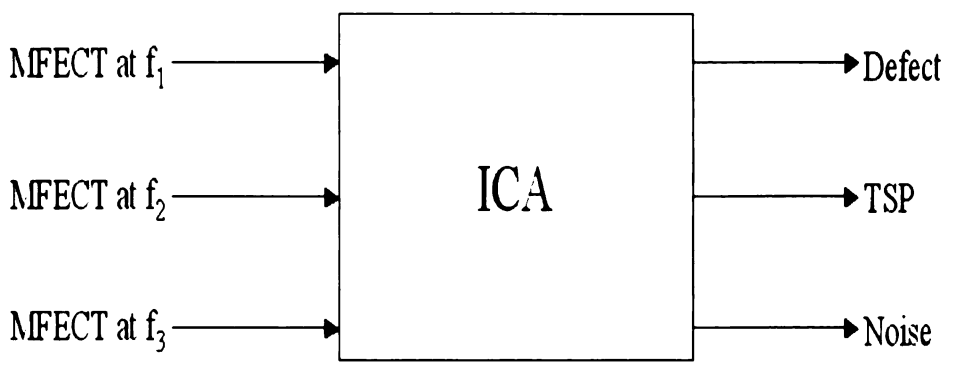

Figure 4.1 Application of ICA to NDT

In order to apply ICA to steam generator tube inspection problem, there is one essential requirement in that the number of ECT measurements should be equal to or more than the number of expected source components. In this study, the measured signal is assumed to be made up of 3 components namely, defect, TSP and noise. Since there are 3 sources to be estimated, it is necessary to have at least 3 different measurements. In this application, Multi-frequency Eddy Current Technique (MFECT) is used to obtain the measurements where the probe is excited at 3 different frequencies. Due to skin effect phenomenon, signal at low frequency carries information about defects that are at a larger depth than the high frequency signal that carries only surface information due to the shallow skin depth. The details of this phenomenon were described in chapter 2. Hence, each set of ECT data includes different combinations of the source signals depending on the excitation frequency that enables ICA to separate out the source signals. Figure 4.2 illustrates the schemes proposed method in this thesis.

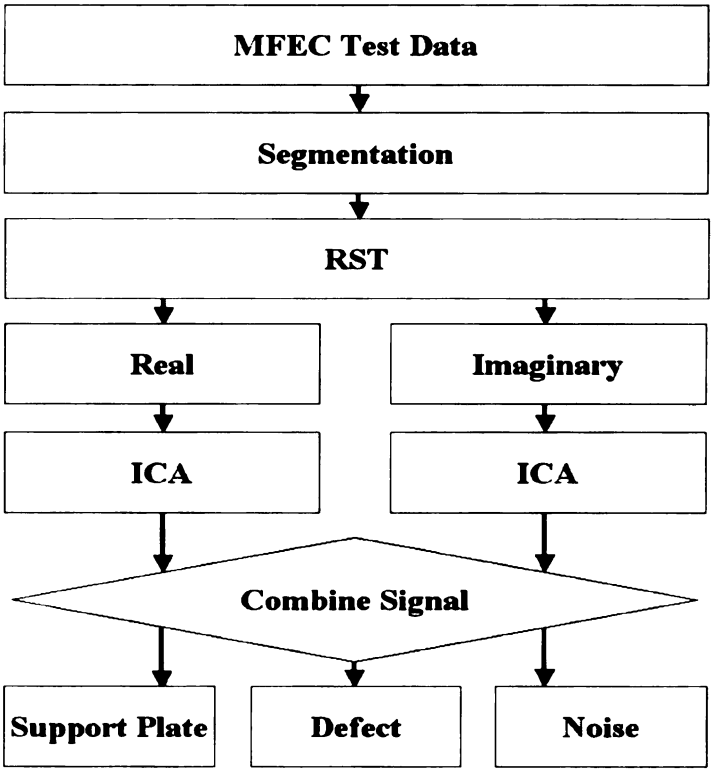

Figure 4.2 Schematic diagram of ICA analysis in NDE

In Figure 4.2, the overall scheme consists of 4 stages. Prior to using MFECT data in the ICA algorithm, they are tuned to a common frequency by means of the rotating, scaling and translation (RST) transform described in section 2.5.2.

1. Segmentation:

In steam generator tube inspection, the probe is pulled through the entire tube resulting in a large amount of data that typically includes multiple TSPs and defects. The ECT signals are calibrated and preprocessed to extract segments of signals with single indication typically at the TSP locations. Consequently, each of these segments can contain contribution from TSP alone or TSP and defects or TSP, defect and noise. These signals are then applied to the ICA algorithm. The MFECT data collected are segmented

to include contribution of a defect and tube support plate (TSP).

2. Signal Transformation:

Rotating, scaling and translation (RST) transformation is applied to the segmented MFECT data. RST transforms a low frequency eddy current data to corresponding high frequency signal. The RST parameters, such as rotating angles, scales and translation parameters, are obtained from the calibrated standard ECT data. The result of RST transformation is given below. Figure 4.3 shows the result of RST transform applied to ECT data at 200㎑. The transformed signal is compared to the signal predicted when the excitation frequency is 400㎑.

3. ICA algorithm:

After MFECT data sets are transformed using RST, ICA is applied separately to the real and the imaginary parts of MFECT data. As a result of ICA, the real and imaginary parts of component source signals are estimated. The real part and the imaginary part of the same component – defect, TSP or noise – can then be combined to estimate the impedance trajectory of the defect and TSP.

4. Combine the extracted signals that are a similar distribution to produce the impedance plane trajectory of the estimated signal.

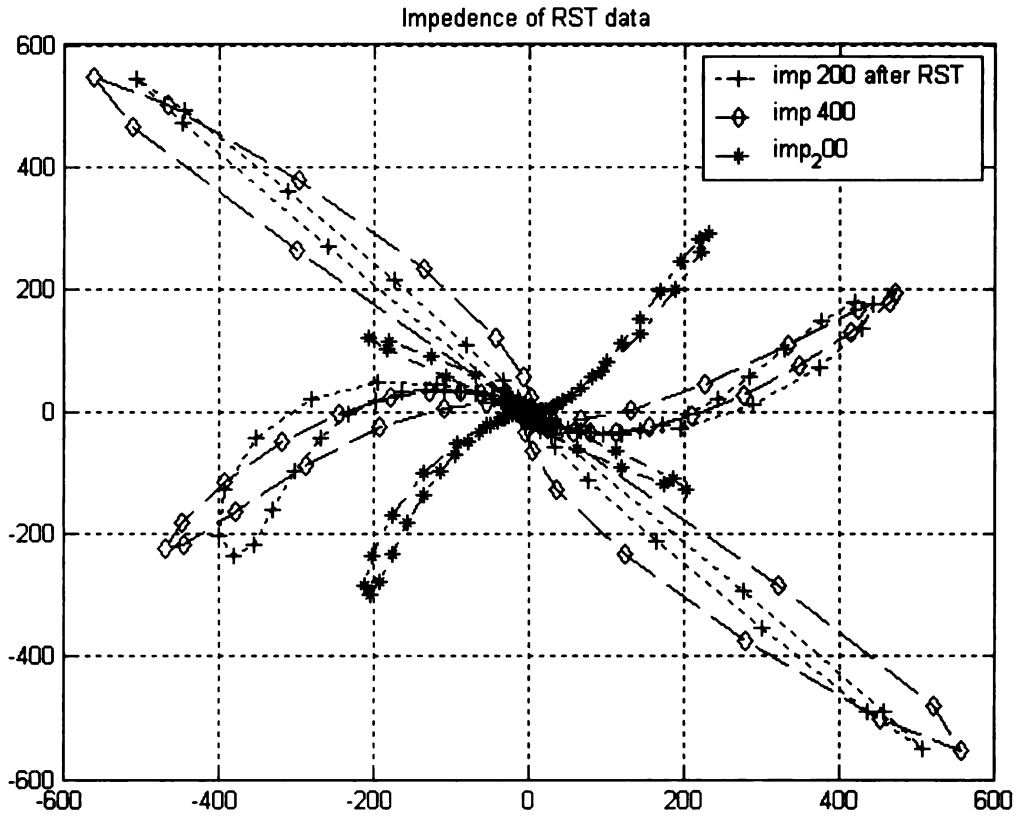

Figure 4.3 Impedance trajectory plots of ECT data after RST

4.2. Finite Element Method (FEM)

For evaluating the performance of ICA algorithm, simulated MFECT data were obtained from a theoretical model that was used to generate ECT signal with TSP and defect parameters. Finite element method (FEM) has been widely used for solving the governing partial differential equations underlying physical process. Analytical, numerical and hybrid methods have been in existence for solving the governing equations. Finite element method is based on the principles of variational calculus. The solution to the governing differential equation involves the incorporation of the equation in an

integral form using energy functional. The energy functional, which represents the energy of the system whose stationary value is a minimum, is minimized resulting in the solution to the governing equation.

The geometry consists of an infinitely long tube within which moves a probe as seen in Figure 4.4. The axisymmetric nature of the current source and the vector potential allows the reduction of the problem to the two-dimensional plane and a coarse finite element mesh spanning the region is given in Figure 4.5. The finite element method consists of following steps.

1. The region of interest is discretized with a suitable mesh consisting of a number of elements connected at the common nodal points as shown in Figure 4.5.
2. The node and the elements of the different materials in the regions are identified and numbered.
3. An interpolating function, which approximates the continuous field over each element in terms of the nodal point value is defined in such a way that the field is continuous across the element boundaries. The interpolating function can be linear or nonlinear and depends on the variations of the field in the test geometry.
4. Minimization of the energy functional with respect to the unknown nodal point values results in a matrix equation.
5. The solution of the matrix equation yields the field values in the region of interest.

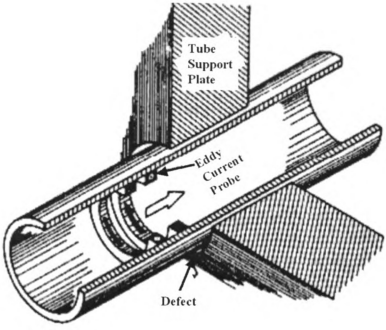

Figure 4.4 Geometry for eddy current NDT [34]

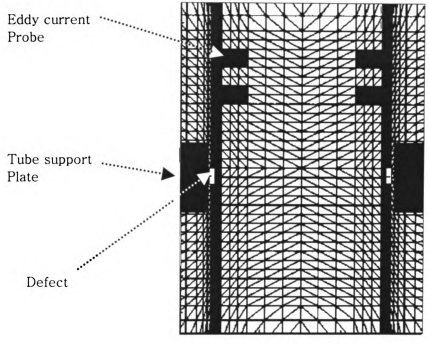

Figure 4.5 A finite element mesh for eddy current geometry

The finite element formulation in terms of magnetic vector potential $\mathbf{A}$ for the two dimensional axisymmetric eddy current phenomena was developed by Lord and Palanisamy [35]. Once the magnetic vector potential values at all the nodes in the mesh region are determined, the probe impedance that is our parameter of interest can be computed. Two different approaches commonly used to estimate this value, are the direct and energy methods and are described in more detail next.

Direct Method

The impedance of a single turn coil of radius r carrying an alternating current of I_s amperes is given by

$$\mathbf{Z} = \frac{\mathbf{V}}{\mathbf{I_s}} \tag{4.1}$$

where $\mathbf{V}$ is the RMS phasor voltage induced in the coil, expressed in terms of the electric field intensity $\mathbf{E}$ as

$$\mathbf{V} = -\int_C \vec{\mathrm{E}} \bullet \vec{dl} \tag{4.2}$$

From equation (2.13), we have

$$\mathbf{E} = -\frac{\partial \mathbf{A}}{\partial t} - \nabla \phi \tag{4.3}$$

Assuming that the field varies harmonically with frequency w given by the equation

$$\mathbf{A} = \mathbf{A}_0 e^{-jwt} \tag{4.4}$$

we have

$$\mathbf{E} = -jw\mathbf{A} - \nabla \phi \tag{4.5}$$

Since the induced voltage is independent of the gradient of the scalar potential $\nabla\phi$, substituting equation (4.5) into (4.2)

$$\mathbf{V} = -jw\int_C \mathbf{A}\, dl \tag{4.6}$$

From equation (4.1), the impedance of the coil is

$$\mathbf{Z} = \frac{jw}{\mathbf{I_s}}\int_C \mathbf{A} dl \tag{4.7}$$

which for a single turn coil of radius r is

$$\mathbf{Z} = j\frac{2\pi wr\mathbf{A}}{\mathbf{I_S}} \tag{4.8}$$

The real and imaginary part of which can be interpreted as the resistive and reactive components of the impedance.

The coil impedance however is calculated in an approximate manner using the finite element method. Consider the cross-section of the coil, discretized by triangular elements. If the dimensions of the elements are small than the vector magnetic potential of all the turns covered by the element i can be approximated by the centroidal value $\mathbf{A}_{ci}$ and similarly the radius of all the turns in the element can be approximated by the centroidal value r_{ci}. From equation (4.8), the impedance for each turn within the element i is given by

$$\mathbf{Z} = j\frac{2\pi wr_{ci}\mathbf{A}_{ci}}{\mathbf{I_S}} \tag{4.9}$$

If N_S is the total number of turns in the coil cross-section, N_t turns/m^2, the turn density of the element and a_i the area of the element, the total impedance of all the turns in the element i is given by

$$\mathbf{Z} = j\frac{2\pi w r_{ci}\mathbf{A}_{ci}a_i N_t}{\mathbf{I_S}} \tag{4.10}$$

If the number of elements in the cross-section of the coil is N_C, the total impedance is

$$\mathbf{Z} = j\frac{2\pi w r_{ci}\mathbf{A}_{ci}}{\mathbf{I_S}}\sum_{i=1}^{N_c} a_i r_{ci}\mathbf{A}_{ci} \tag{4.11}$$

The coil impedance in a two dimensional or axisymmetric problem can be computed using the method explained here. This method assumes that the magnetic vector potential values are constant along the source, i.e. along the circumferential direction of the coil. However, this is not true in the case of 3-dimensional problems. An alternate method to compute the impedance based on the calculation of the stored and dissipated energies is explained next.

Energy Method

The impedance of a coil can be calculated from the energy of the system since the inductance and the resistance are associated with the stored and dissipated energies, in the system, respectively. The stored energy E is given by

$$E = \frac{1}{2}\int_v \vec{\mathbf{B}} \bullet \vec{\mathbf{H}}\, dv \tag{4.12}$$

From equation (4.12) assuming constant reluctivity in each direction the energy stored in a finite element of volume V_i can be written in terms of B as

$$E_i = \frac{1}{2}\left(v_x B_x^{\,2} + v_y B_y^{\,2} + v_z B_z^{\,2}\right)V_i \tag{4.13}$$

where v_x, v_y and v_z are the reluctivities in the corresponding directions.

From the relation between the magnetic flux density and vector magnetic potential

$\vec{B}$ we have

$$B_x = \frac{\partial A_z}{\partial y} - \frac{\partial A_y}{\partial z}$$
$$B_y = \frac{\partial A_x}{\partial z} - \frac{\partial A_z}{\partial x} \qquad (4.14)$$
$$B_x = \frac{\partial A_y}{\partial x} - \frac{\partial A_x}{\partial y}$$

Substituting this in equation (4.13) and adding all the elements in the mesh region, the total stored energy in the system is given by

$$E = \sum_{i=1}^{N}\left[v_x\left(\frac{\partial A_{zi}}{\partial yi} - \frac{\partial A_{yi}}{\partial zi}\right)^2 + v_y\left(\frac{\partial A_{xi}}{\partial zi} - \frac{\partial A_{zi}}{\partial xi}\right)^2 + v_z\left(\frac{\partial A_{yi}}{\partial xi} - \frac{\partial A_{xi}}{\partial yi}\right)^2\right] V_i \qquad (4.15)$$

The inductance of the coil can then be calculated using

$$E = \frac{L I_S^{\,2}}{2} \quad \text{or} \quad L = \frac{2E}{I_S^{\,2}} \qquad (4.16)$$

where I_S is the current in the source coil.

The resistance of the coil is associated with the dissipated energy in the system. The dissipated energy in a finite element of volume V_i is given by

$$P_i = \frac{V_i \left| J_{eddy} \right|^2}{\sigma} \qquad (4.17)$$

where J_{eddy} is the eddy current density and was derived in chapter 2 as

$$J_{eddy} = -jw\sigma A_{ci} \qquad (4.18)$$

where A_{ci} is the centroidal magnetic vector potential value for the element i.

Substituting equation (4.18) into (4.17) and summing all the elements in the mesh

region, the total dissipated energy is given by

$$P = \sum_{i=1}^{N} P_i = \sum_{i=1}^{N} V_i \sigma w^2 |A_{ci}|^2 \tag{4.19}$$

Using $P = I^2R$, the resistance of the coil is given by

$$R = \frac{P}{I^2} \tag{4.20}$$

and the coil impedance is

$$Z = R + jwL \tag{4.21}$$

The above formulation is applicable to two dimensional and axisymmetric problems. By definition the total flux linkages in a coil with N_S turns is equal to $N_S\phi$ where ϕ is the flux linkages due to a coil with 1 turn. Multiplying the corresponding values of the magnetic flux density and the vector potential value by N, we have the impedance of the coil with N_S turns to be

$$Z_N = N_S^2 Z \tag{4.22}$$

where Z is the impedance of the coil with 1 turn.

Flux Density and Eddy Current Density

Once the vector magnetic potentials are computed, the formulations of the flux and eddy current densities for the axisymmetric two-dimensional case are obtained as

$$\begin{aligned} B &= \nabla \times A \\ J_{eddy} &= -jw\sigma A \end{aligned} \tag{4.23}$$

where B is the flux density and J_{eddy} is the eddy current density.

5. SIMULATION RESULTS AND DISCUSSIONS

The proposed ICA algorithm was first applied to synthetic data obtained from the finite element model (FEM) and then on experimental data collected from the steam generator tubes in a nuclear power plant. The function of the source signals separation from the observed multi-frequency eddy current (MFEC) data is focused as the essential feature of ICA. However, application of ICA for noise filtering is also tested. Fast-ICA algorithm and preprocessing are employed to extract the original signals from MFEC data. For the FEM simulations, only defects, support plates and noise are considered as source components. For 3 distinct sources, we need at least three sets of MFEC data at different excitation frequencies. Hence, FEM simulation of MFEC inspection process was conducted at three excitation frequencies, namely, 35kHz, 200kHz and 400kHz. Due to the property of ICA, the sign or scale is not guaranteed for the extracted source signal. Hence, the sign or scale has little meaning at the result. Instead, the distribution of signal gives information about the extracted source signals.

Two sets of results were obtained from implementation of ICA on FEM data. The first set of results considered a defect in a support plate region at 35kHz and 400kHz and the second set of results evaluates the performance of ICA in filtering noise as well as separating source signals. For evaluating noise filtering, random white noise (2 dB SNR with 50 dB of signal power) is added to ECT data. The noise component is assumed to be the same at each excitation frequency. ECT data at 35kHz, 200kHz and 400kHz are used as input to ICA and three source signals due to defect, support plate and noise, are extracted as output. In addition, the signal to noise ratio of the extracted flaw signal is seen to be

significantly higher, indicating that ICA can be used to denoise data. These results are shown in section 5.1.

The ICA algorithm was also applied to MFEC field data collected at excitation frequencies of 35klz, 200klz, 400klz and 600klz. The MFEC field data and the corresponding results are shown in section 5.2.

5.1. Simulation of FEM Data

The finite element model allows us to obtain signal under controlled conditions of defect geometry, excitation frequency and material properties. The geometry including support plate and defect is shown in Figure 4.5. Table 1 shows the value of the parameters used in the model. The real and imaginary components of the probe impedance for the geometry in Figure 4.5 at frequencies 35klz, 200klz and 400klz are shown in Figure 5.1, 5.2 and 5.3, respectively.

Category	Electirical Conductivity $(ohm\text{-}meter)^{-1}$	Relative Permeability (μ)	Current Density (A/m^2)
Tube	1×10^6	1	-
Support Platel	10×10^6	10×10^6	-
Coil	0	1	10^6

Table 5.1 Parameters for Finite Element Model

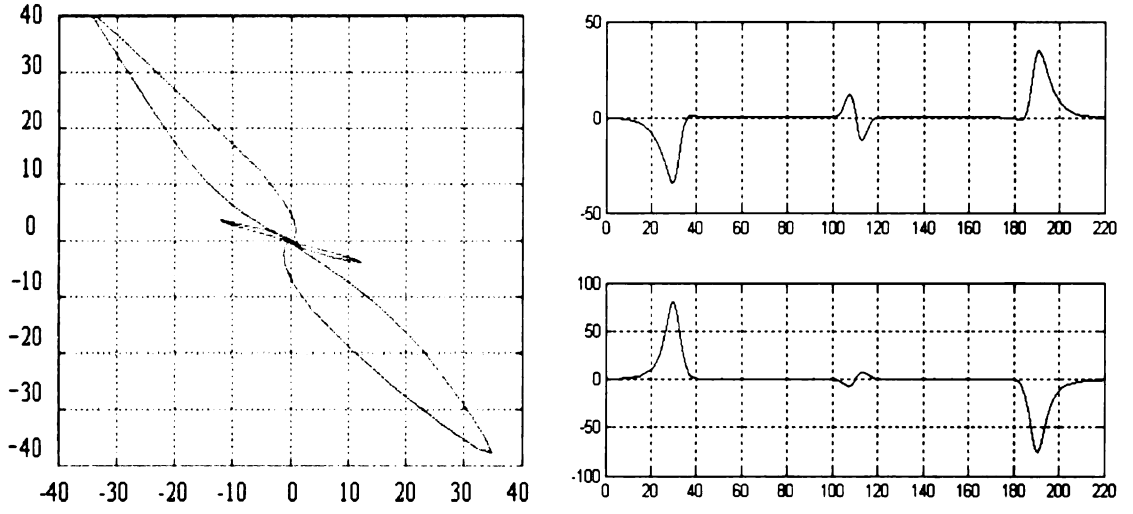

Figure 5.1 ECT data from FEM at frequency of 35 kHz (a) Impedance trajectory (b) Real component of eddy current signal (upper) and imaginary component of eddy current signal (lower)

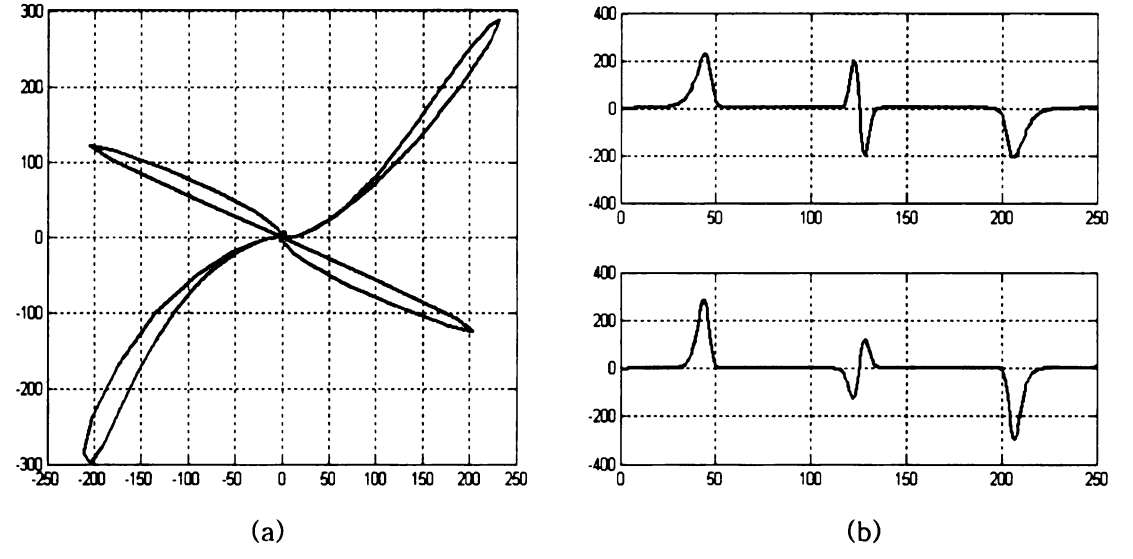

Figure 5.2 ECT data from FEM with excitation frequency of 200 kHz (a) Impedance trajectory (b) Real component of eddy current signal (upper) and imaginary component of eddy current signal (lower)

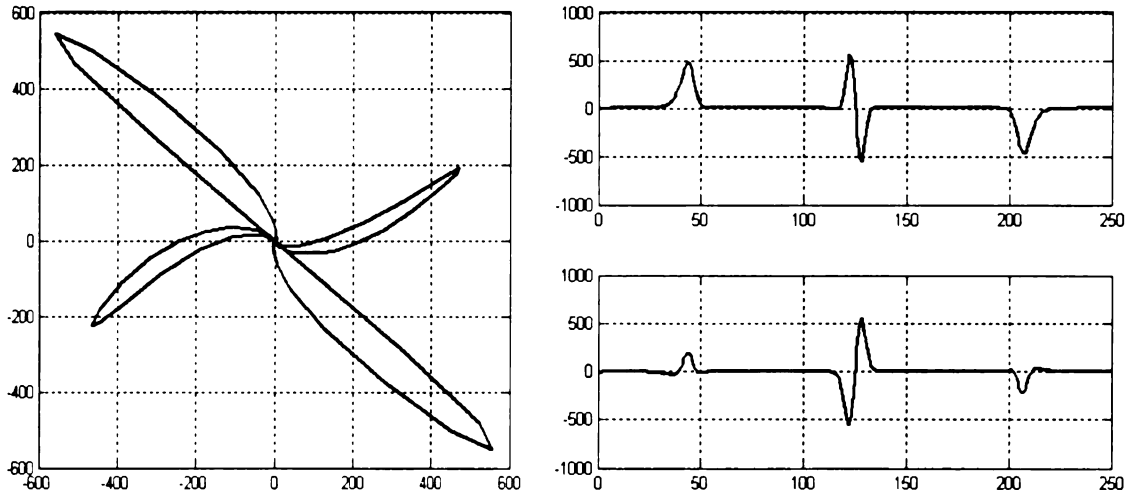

(a) (b)

Figure 5.3 ECT data from FEM with excitation frequency of 400 kHz (a) Impedance trajectory (b) Real component of eddy current signal (upper) and imaginary component of eddy current signal (lower)

5.1.1. Source Signals Separation (Defect and TSP)

The main objective of ICA is to extract defect signal from multi-frequency eddy current (MFEC) data in the presence of signals from external structures such as TSP, tube sheets (TS) and conductive deposits in addition to the flaws in the tube. The purpose of this simulation is to evaluate the ability of ICA to separate out the defect information from the irrelevant signals from other components using ECT data generated by finite element model (FEM), which is noise-free. MFEC data at 35kHz and 400kHz are shown in Figure 5.1 and 5.3, respectively. The real part (horizontal component) and the imaginary part (vertical component) of ECT data are considered separately, processed by ICA and reassembled to construct impedance trajectories of source components. The real part and imaginary part of MFEC signals at 35kHz and 400kHz are shown in Figure 5.5 where the two

indications at the end correspond to support plates and the indication in the middle is generated from the defect. Reconstructed defect signal and support plate signal are shown in (c) and (d) along with the corresponding impedance plot. The impedance trajectories of the defect and the support plate signal extracted from mixed MFEC data are shown in (c) and (d) in Figure 5.4.

In the mixing algorithm described in chapter 2, the "mixed" signal still contains some residual signal at the origin indicating that the effect of support plate is not completely removed. However, the relevant source information due to the defect extracted from the mixed signal using ICA allows distinguishing the defect information without any contribution from the TSP. The real and imaginary components of data are shown in Figure 5.5.

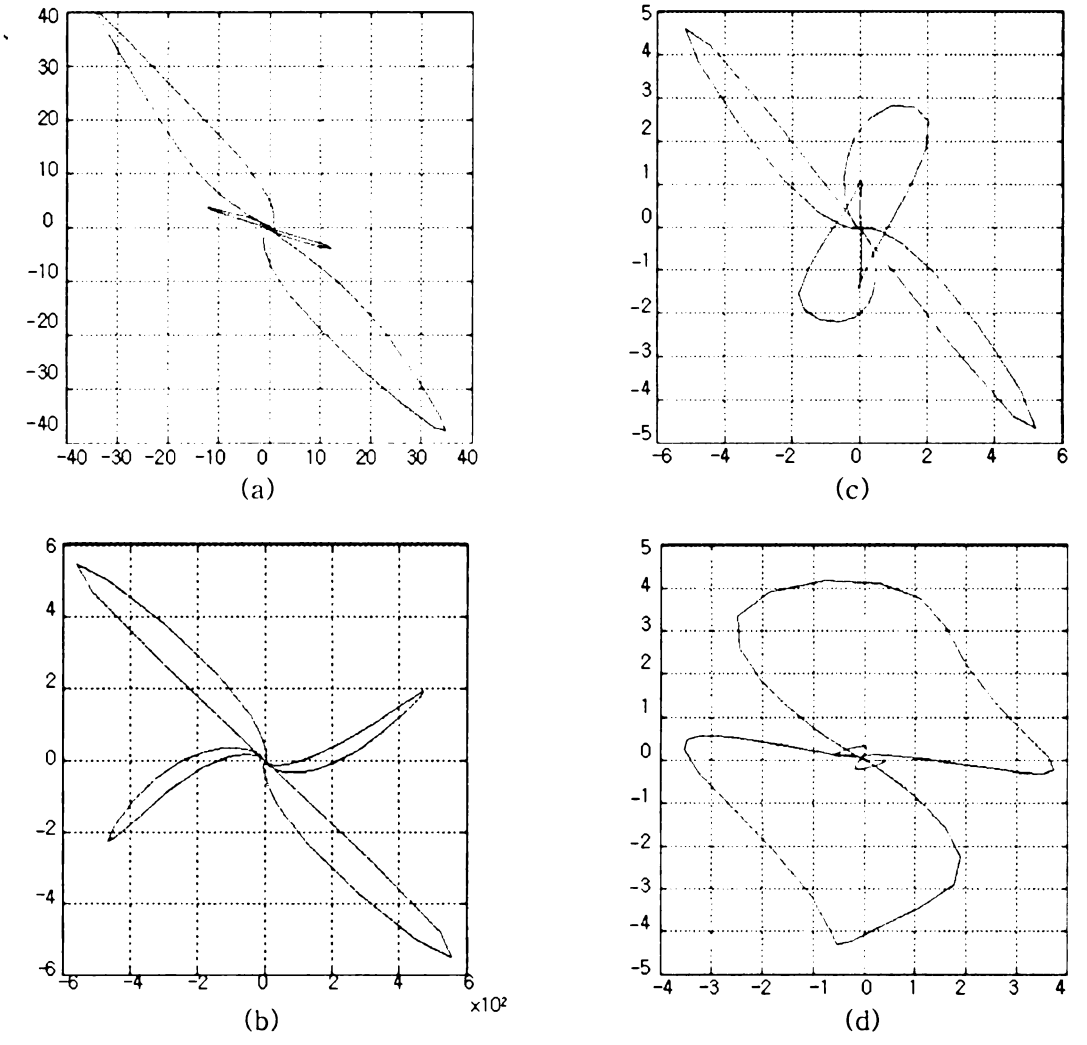

Figure 5.4 Impedance trajectories using FEM at (a) 35 kHz (b) 400 kHz (c) separated defect signal (d) separated support plate signal

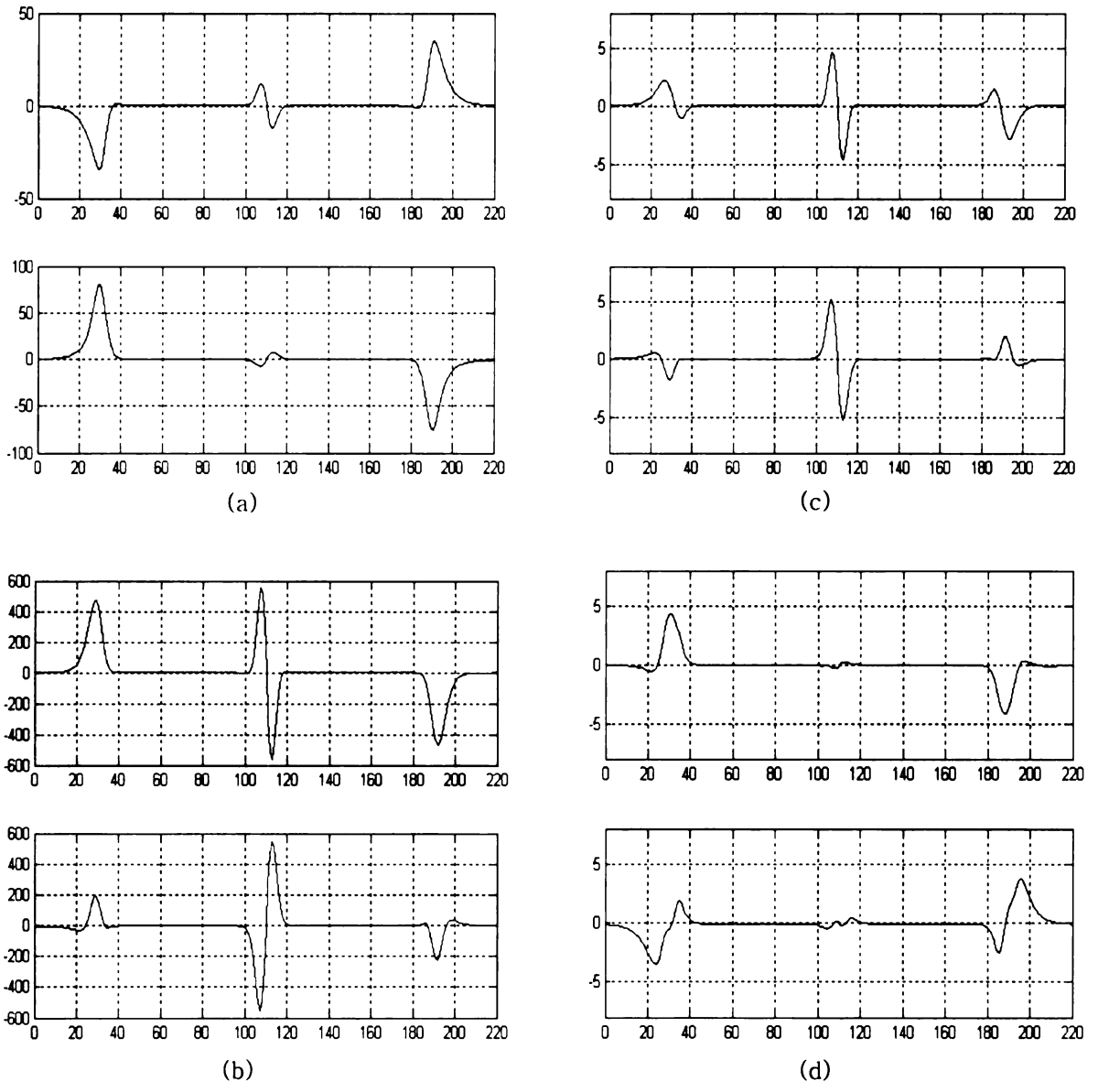

Figure 5.5 Real component (Upper) and imaginary component (Lower) of (a) FEM–ECT signals at 35 kHz (b) FEM–ECT signal at 400 kHz (c) extracted defect signal (d) extracted support plate signal

5.1.2. Source Signals Separation (Defect, TSP and Noise)

The purpose of this simulation is to evaluate the ability of ICA to function as a noise filter as well as source separator. ECT data is often corrupted by the presence of noise or interference signals depending on inspection conditions. Sometimes, defect signal is buried in noise signal which makes it difficult to extract meaningful defect information from the measured ECT data. This section describes the use of ICA to remove noise. Usually noise is modeled by a Gaussian distribution which violates one of conditions for ICA. However, when there is only one component that has Gaussian distribution, residue theory [36] can be employed to filter out Gaussian noise from observed ECT signals.

The ECT signal generated by finite element model (FEM) at excitation frequencies of 35 kHz , 200 kHz and 400 kHz are corrupted by adding random white noise signal (2 dB SNR with 50 dB of signal power) to each data set. The noisy signal is input to ICA which produces 3 separated source signals. These results are shown in Figure 5.6. Figure 5.7 shows noisy version of the horizontal (real) and vertical (imaginary) components of FEM-ECT data in (a) and (b), respectively. The resulting source signals due to – defect, support plate and noise – are extracted and shown as impedance trajectories in Figure 5.6. The result shows that source components – defect, support plate and noise are successfully extracted from noisy ECT measurements.

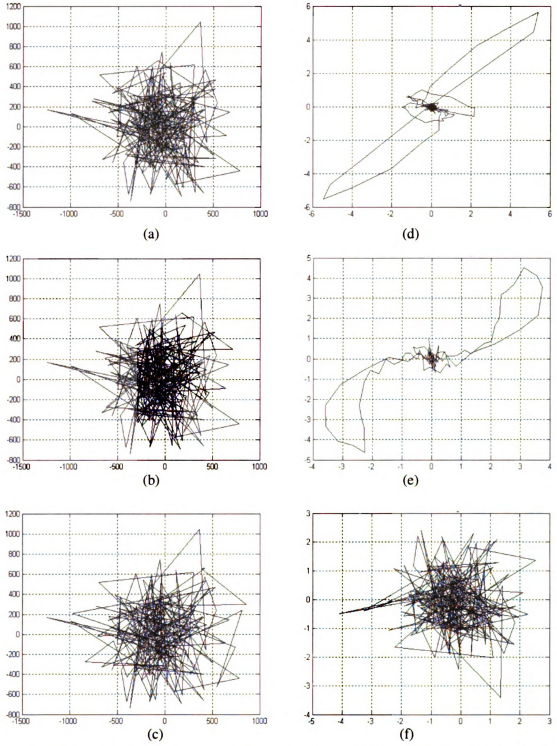

Figure 5.6 Source signal separation with noise filtering (simulated trajectories): (a) Noisy ECT data at 35 kHz, (b) Noisy ECT data at 200 kHz, (c) Noisy ECT data at 400 kHz, (d) Separated Defect Signal, (e) Separated Support Plate Signal, (f) Separated Noise

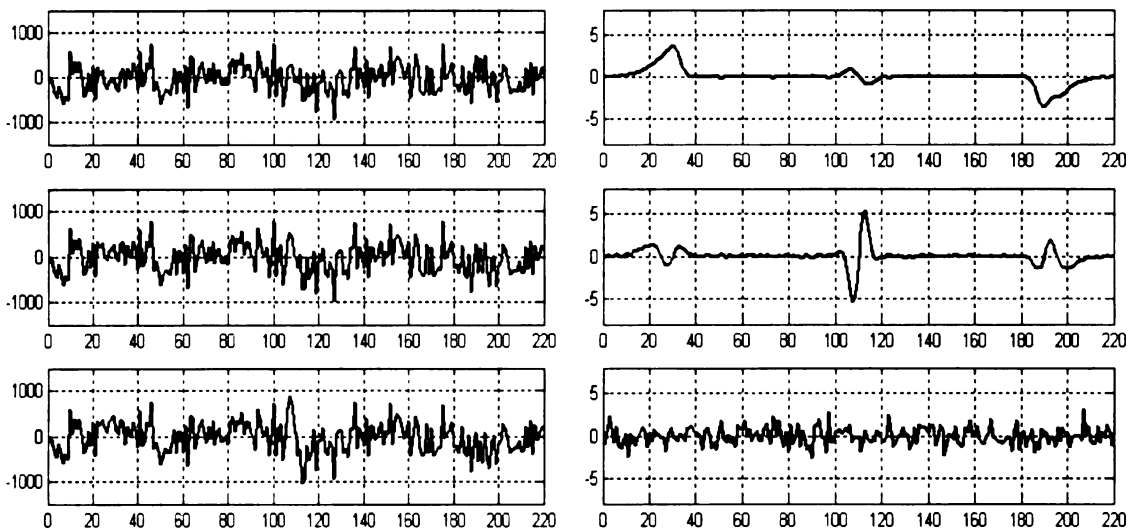

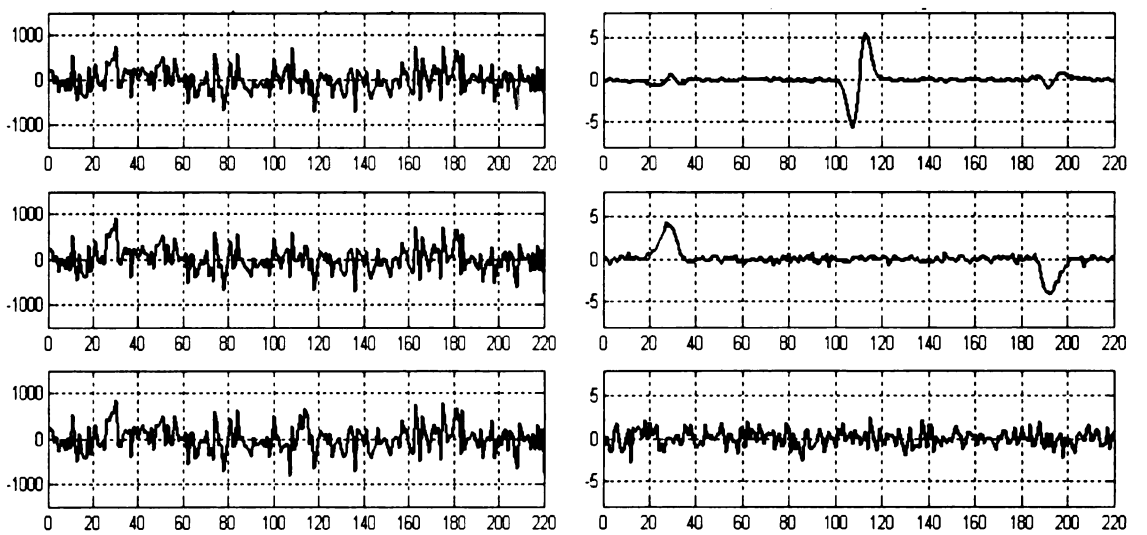

Figure 5.7 Source signal separation with noise filtering (simulated data): (a) noisy horizontal ECT data at 35 kHz (top), 200 kHz(middle) and 400 kHz(bottom), (b) noisy vertical ECT data at 35 kHz (top), 200 kHz(middle) and 400 kHz(bottom), (c) separated signals (horizontal component), (d) separated signal (vertical component)

5.2. Performance on Experimental Data

While the synthetic ECT data is obtained from finite element model (FEM), the experimental data are collected during inspection of steam generating tubes. In fact, a variety of operational parameters and material conditions such as lift-off, local variations in permeability, conductivity and material composition, surface roughness, etc. give rise to a noisy signal, which makes the detection of the true defect signals a formidable task.

The impedance signals from the EC probe are measured at 4 excitation frequencies – 35kHz, 200kHz, 400kHz and 600kHz. The maximum number of components that can be estimated is equal to the number of available data sets. Hence, at most 4 source components can be estimated. In this test, 3 source components are assumed, namely defect, support plate and noise. In the preprocessing stage, rotation, scaling and translation (RST) parameters are obtained from the calibration standard as described in 2.5.2 and 4.1.

5.2.1. Extraction of the Defect Signal from Mixture of Defect and Noise

ECT field data obtained from Nuclear Power Plant (NPP) SG tube inspector was used in this test. Figure 5.8 (a) presents a set of 4 horizontal channel EC signals obtained at different excitation frequencies – 35kHz, 200kHz, 400kHz and 600kHz. Preprocessing using RST transformation is first applied to the signals to transform all signals to match the corresponding signal at 600kHz. The parameters for RST are obtained from the standard calibration. The RST processed signals are applied as input to the ICA algorithm. Figure 5.8 (b) shows 4 independent components extracted as a result of ICA. The first separated horizontal signal has a big pulse at the corresponding defect location (77~85) in the top

figure as indicated. The signal at bottom of Figure 5.8 (b) is regarded as horizontal component of noise.

The result of independent component analysis of the corresponding vertical channel signals is shown in Figure 5.8 (b) and (d). In the separated components in Figure 5.8 (d), the defect signal is extracted as the second independent component and the defect location is indicated. Extracted horizontal and vertical channel noise components are the last signals in the bottom of Figure 5.8 (b) and (d), respectively. Figure 5.9 shows the impedance plane trajectories of defect, TSP signal at 35kHz, 200kHz, 400kHz and 600kHz. Figure 5.10 shows the impedance plane trajectories of defect and TSP extracted by ICA algorithm. The result indicates that it is possible to extract defect information from MFECT data by using ICA algorithm.

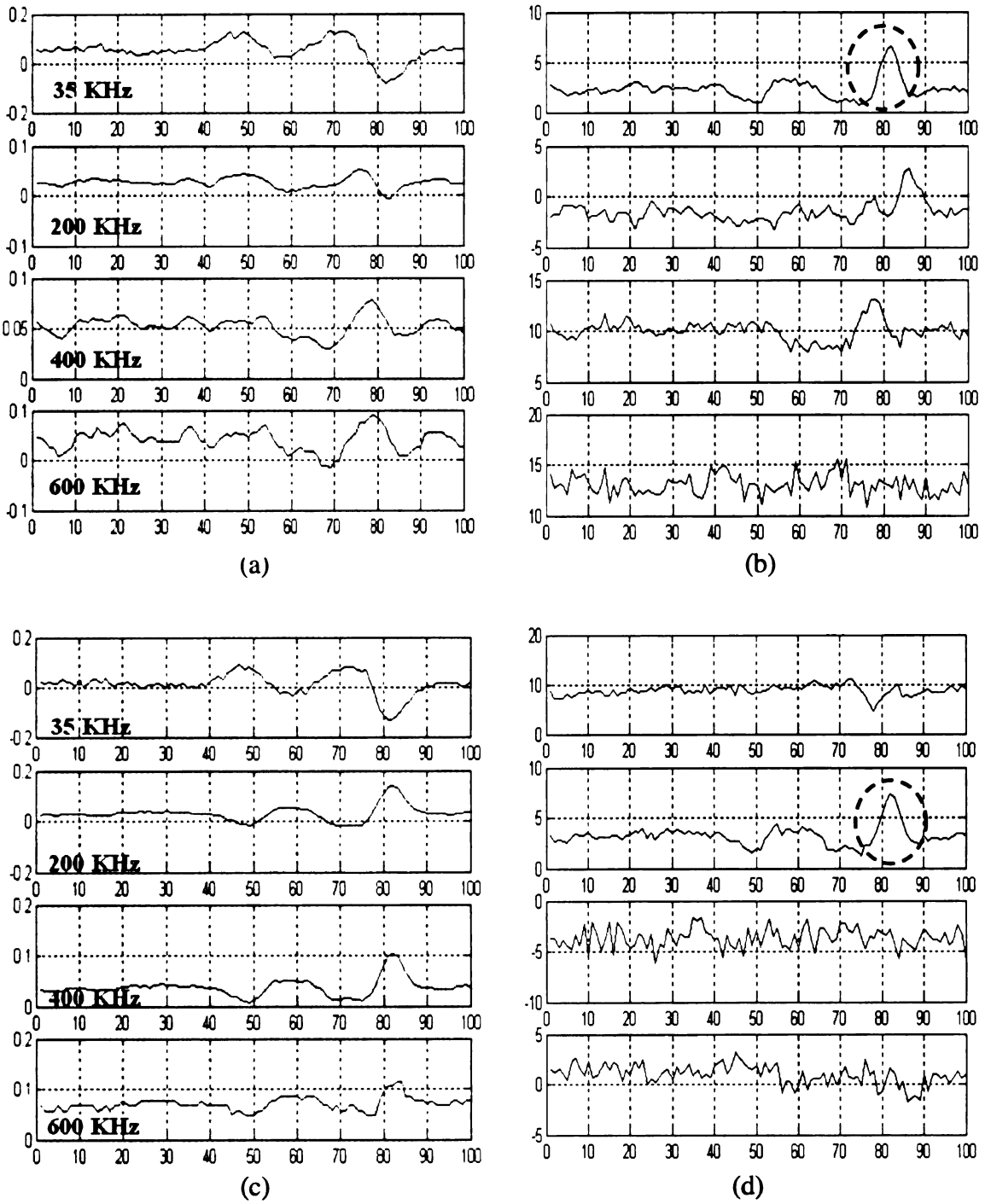

Figure 5.8 Test 1 –ICA implementation with ECT field data: (a) Horizontal ECT data, (b) Horizontal Separated Signal, (c) Vertical ECT data, (d) Vertical Separated Signal

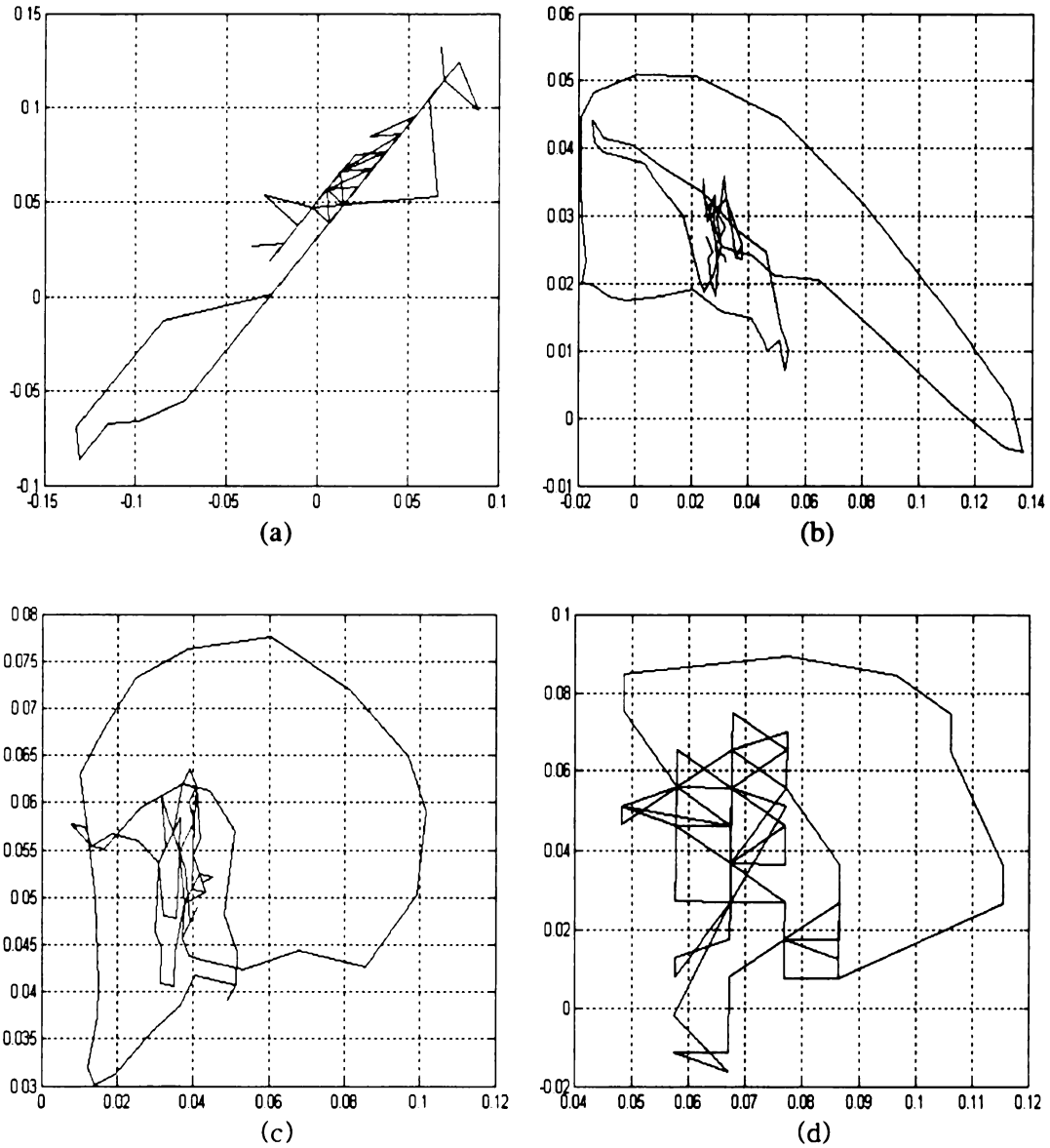

Figure 5.9 Test 1 – Impedance trajectories of ECT field data at frequency: (a) 35kHz, (b) 200kHz, (c) 400kHz, (d) 600kHz

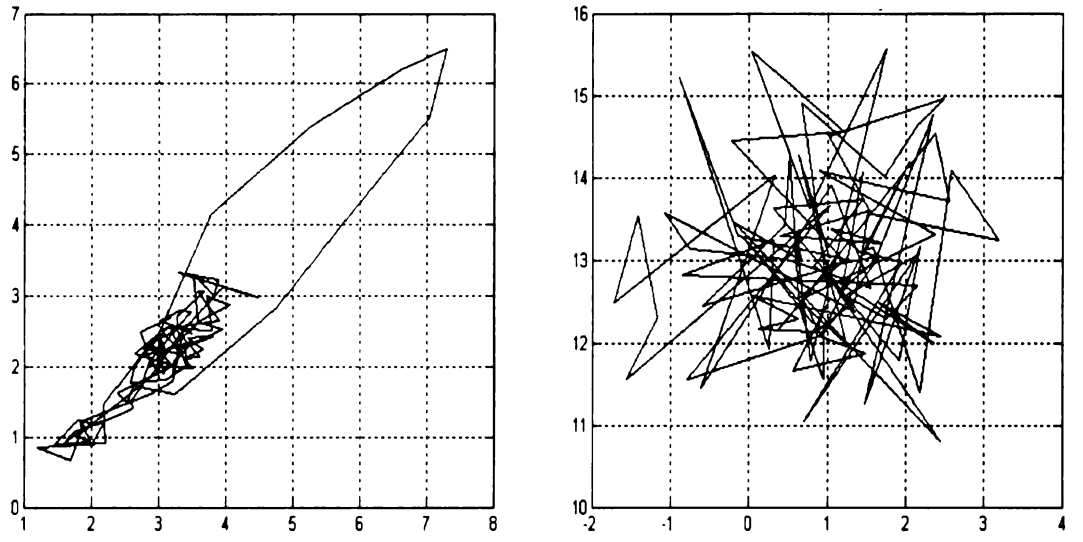

Figure 5.10 Test 1 – Impedance trajectories of the reconstructed signal: (a) Defect, (b) Noise

5.2.2. Extraction of the Source Signal from Defect and TSP

Figures 5.11 (a) and (b) show another example of field data from steam generator (SG) inspection MFECT data at 35kHz, 200kHz, 400kHz and 600kHz. The horizontal channel MFEC data in Figure 5.11 includes a support plate characterized by two pulses at the beginning and at the end of data. The presence of support plate makes it difficult to distinguish defect component from the impedance plane trajectories of MFEC data shown in Figure 5.12.

After preprocessing using RST transformation, the signals are applied to the ICA algorithm. The horizontal components of extracted source signals are shown in Figure 5.11 (b). The first extracted signal is interpreted as the horizontal component of TSP since it exhibits large indication at the location of TSP. The third extracted signal is considered to be the defect signal since it has a big indication at the location of defect. The horizontal or vertical signal of a true defect signal is typically characterized by two spatially separated peaks arising from the two edge points of the defect. The same procedure is implemented

with the vertical components of MFEC data. The vertical channel signals of MFEC data are shown in Figure 5.11 (c) and extracted signals are presented in Figure 5.11 (d). In the signals presented in Figure 5.11 (d), we see that the second signal has a distribution that corresponds to the defect signal. The fourth signal in Figure 5.11 (d) is seen to be that of the vertical component of TSP signal.

The horizontal and vertical signals of defect component yield the impedance plane trajectory shown in Figure 5.13 (a). The impedance trajectory of TSP is presented in Figure 5.13 (b). From the extracted impedance trajectory of defect, we can distinguish that this defect is categorized into wear because the impedance trajectory of defect has only one side loop. Support plate is extracted as another independent component and the impedance trajectory is shown in Figure 5.13 (b).

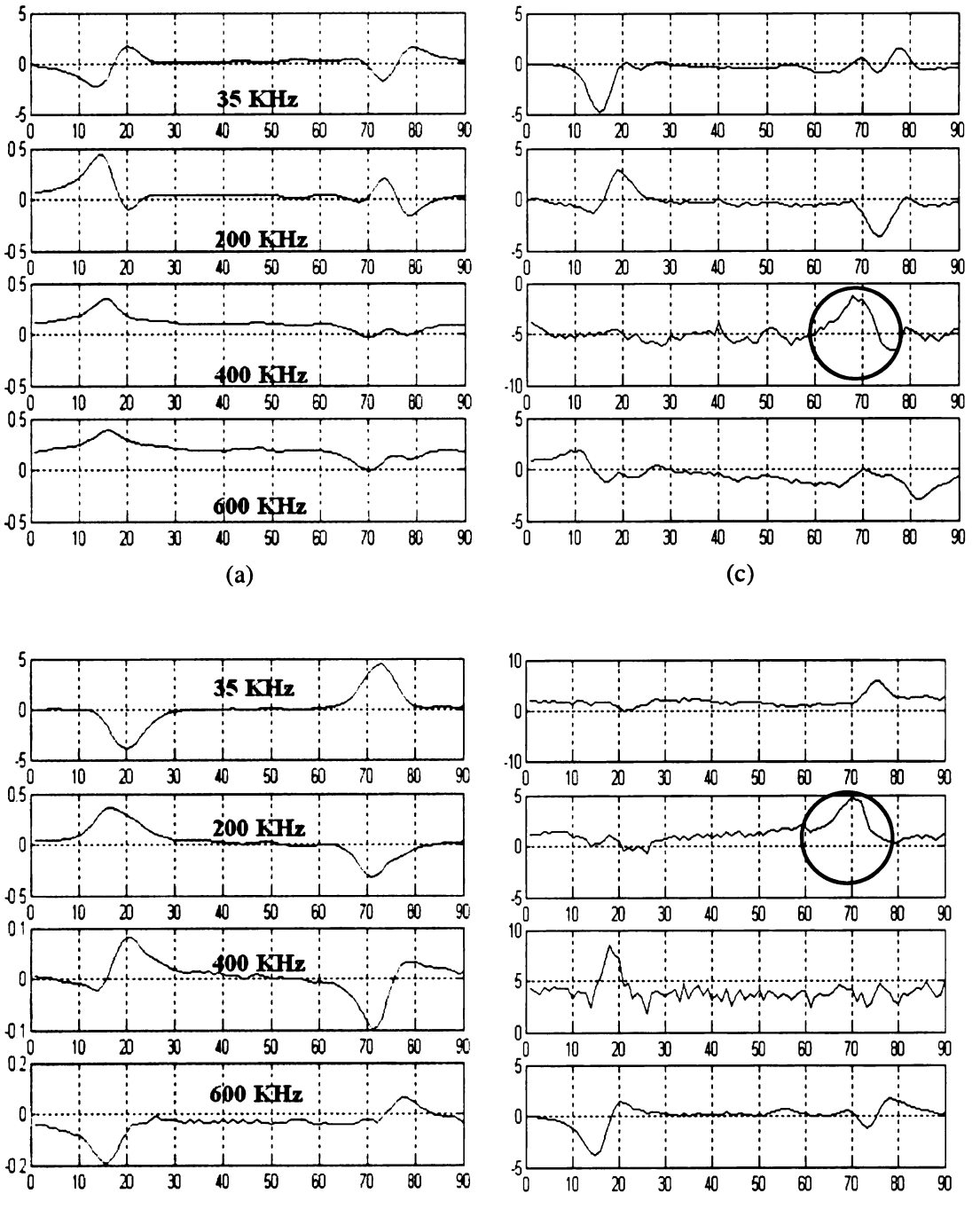

Figure 5.11 Test 2 – ICA implementation with ECT field data: (a) Horizontal ECT data, (b) Vertical ECT data, (c) Separated horizontal signals, (d) Separated vertical signals

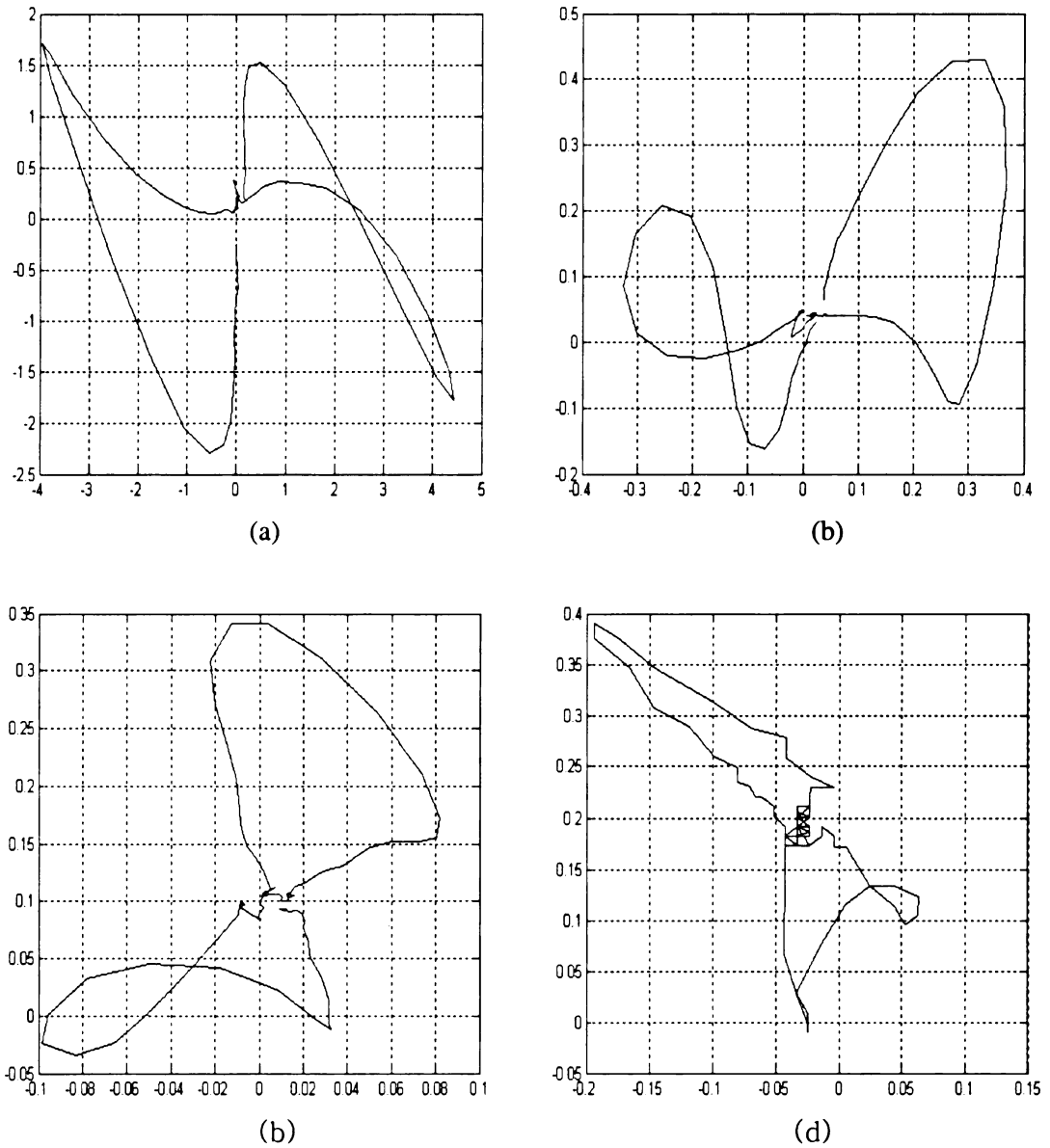

Figure 5.12 Test 2 – Impedance trajectories of ECT field data at frequency: (a) 35kHz, (b) 200kHz, (c) 400kHz, (d) 600kHz

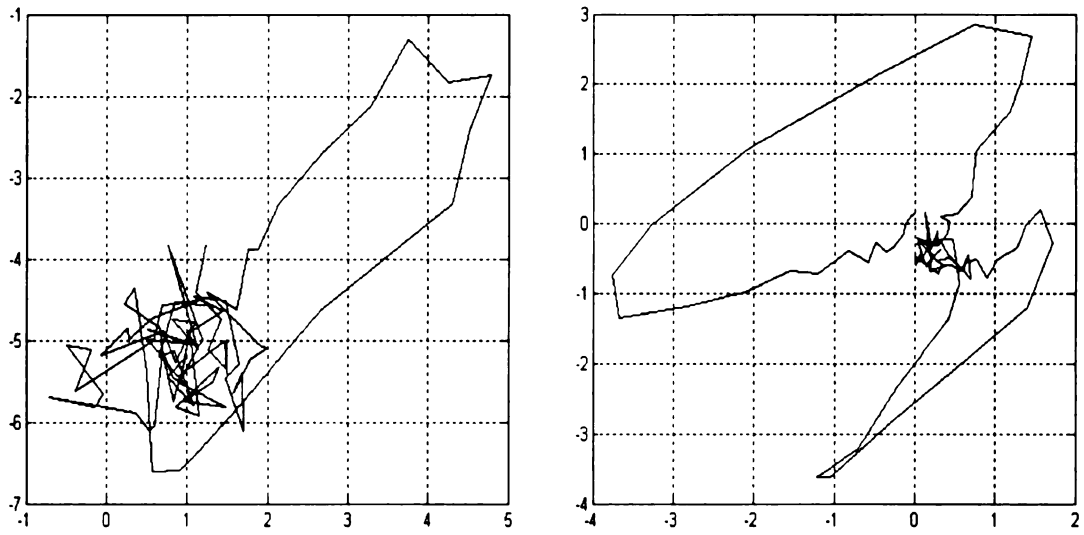

Figure 5.13 Test 2 – Impedance trajectories of the extracted signals: (a) Defect, (b) TSP

5.2.3. Extraction of the Source Signals from Defect and Noise

A third experimental signal from an 'Outside Diameter Inter Granular Attack (ODIGA)' is analyzed next. Figure 5.14 (a) presents the horizontal channel data and resulting source signals are shown in Figure 5.14 (b). The signal at the top of Figure 5.14 (b) is recognized as the defect signal. The third signal is considered to be noise signal. The same procedure is implemented on the vertical channel MFEC data. MFEC data and the extracted signals are shown in Figure 5.14 (c) and (d), respectively. Figure 5.14 (d) shows the defect signal as the second source signal. The third extracted signal in Figure 5.14 (d) is considered as noise signal.

The impedance plane trajectory of MFEC data is shown in Figure 5.15. 4 impedance plane trajectories obtained at different excitation frequencies are presented and it is seen that the defect signal is barely visible. Notice that in contrast to the ideal noise free condition, the

background signal (pertaining to the defect region) has significant amplitude. However, the impedance plane trajectories synthesized from the extracted horizontal and vertical defect signals clearly show the presence of defect in Figure 5.16.

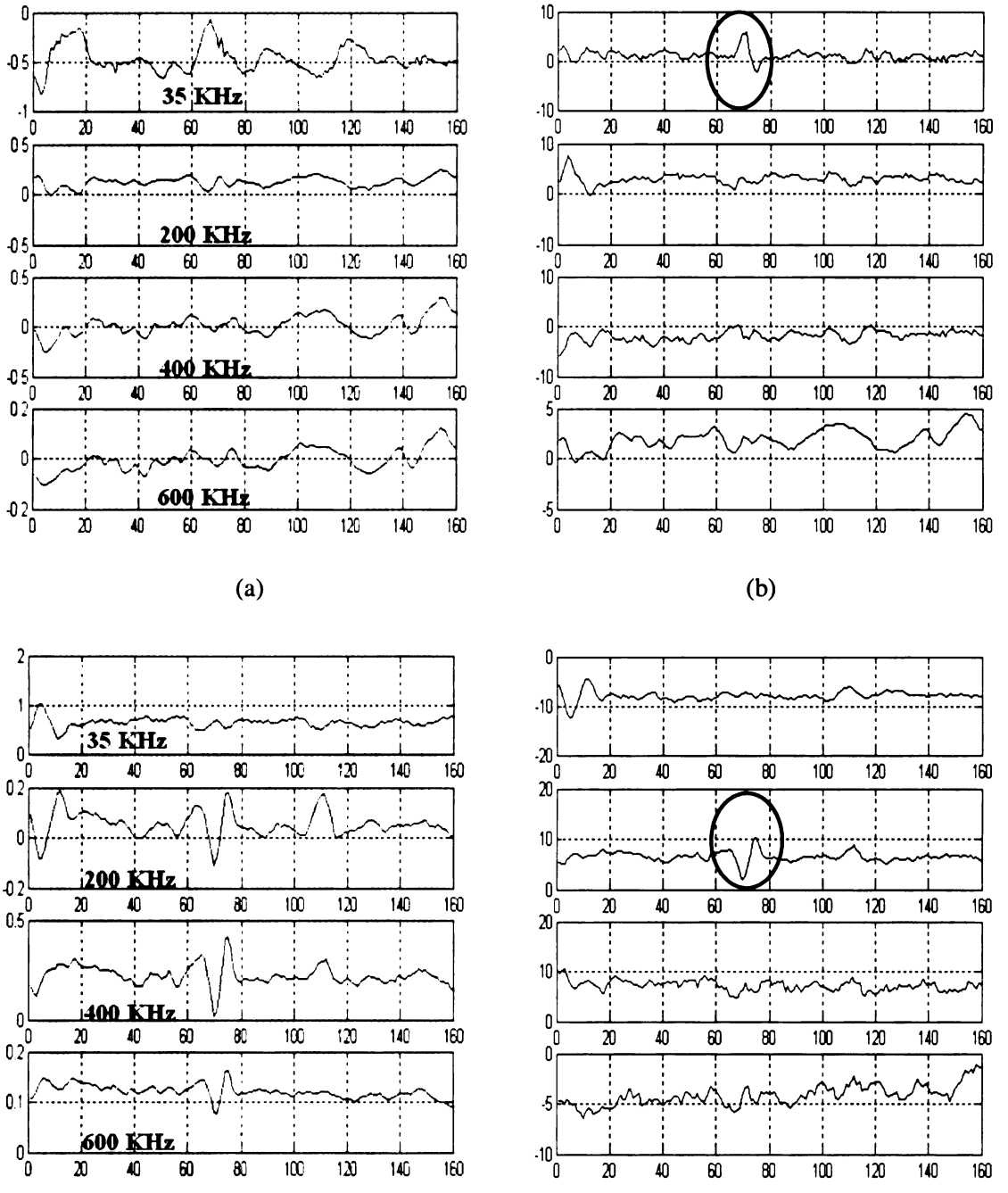

Figure 5.14 Test 3 – ICA implementation with ECT field data: (a) Horizontal ECT data, (b) Horizontal Separated Signal, (c) Vertical ECT data, (d) Vertical Separated Signal

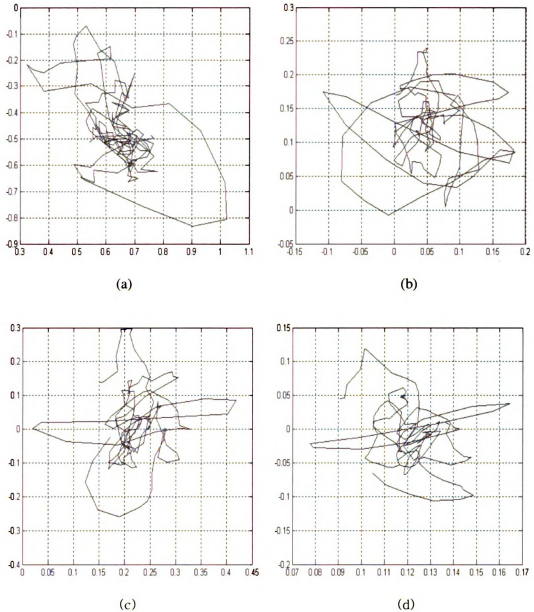

Figure 5.15 Test 3 – Impedance trajectories of ECT field data at frequency: (a) 35kHz, (b) 200kHz, (c) 400kHz, (d) 600kHz

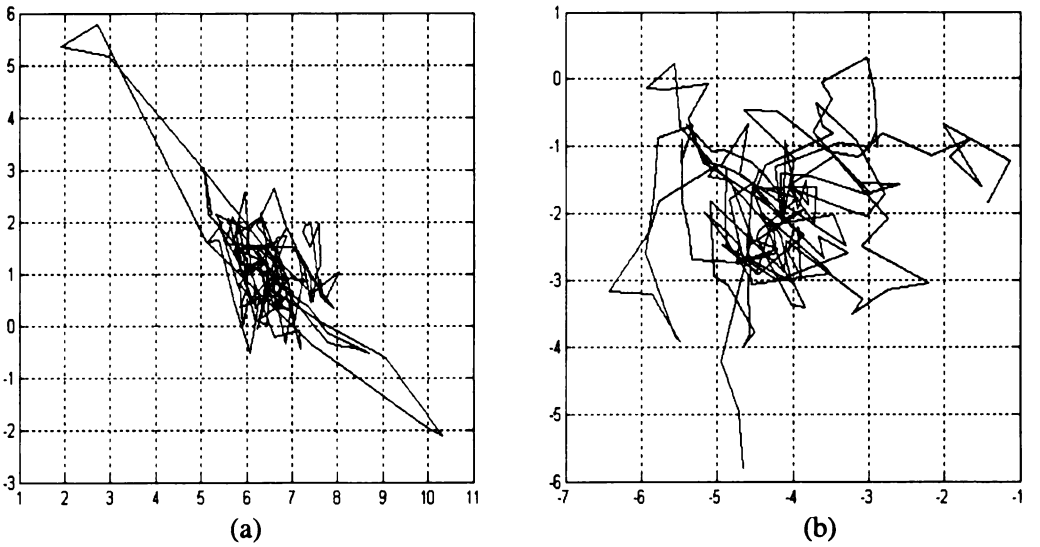

Figure 5.16 Test 3 – Impedance trajectories of the reconstructed signal: (a) Defect, (b) Noise

5.2.4. Use of ICA for defect detector

The ICA algorithm was applied to a database of steam generator (SG) tube inspection signals for the purpose of defect detector. In this experiment, the separated signals are tested for presence of a defect using a criterion function depicted as

$$\mu = \frac{\mathrm{s}[d]}{\mathrm{s}[x]} \tag{5.1}$$

where s[] is standard deviation, x is the entire source signal (100 points) and d is the segment of x at the defect location (15~20 points).

Using μ a decision is made to classify a signal as "defect" or "no defect". The database consists of a total of 110 signals with only TSP and 27 signals comprising TSP and defect. The classification performance is summarized in Table 5.2. The performance showed a detection probability of about 90% (24 out of 27) and probability of false call of about 12% (14 out of 110).

Category	Predicted Detect	Predicted No Defect	Total
True Defect	24	3	27
True No Defect	96	14	110

Table 5.2 Statistics on the ICA performance

In order to compare the performance of ICA with that of conventional mixing algorithm the second database was used for which results obtained using mixing algorithm was available. The performance of ICA and mixing algorithm are summarized in Table 5.3 and Table 5.4, respectively. It can be seen from theses results that ICA performs better than mixing algorithm both in terms of detection probability and number of false calls.

Category	Predicted Detect	Predicted No Defect	Total
True Defect	30	4	34
True No Defect	8	30	38

Table 5.3 Statistics on the ICA performance

Category	Predicted Detect	Predicted No Defect	Total
True Defect	25	9	34
True No Defect	10	28	38

Table 5.4 Statistics on the mixing algorithm performance

6. CONCLUSION AND FUTURE WORK

6.1. Conclusion

The application of ICA in enhancing differential eddy current probe signals from flaws in the vicinity of tube support plate (TSP) in steam generator tubing is evaluated in this thesis. ICA is a general-purpose statistical technique in which observed random data from mixture of sources are decomposed into components that are maximally independent from each other. The proposed Fast ICA algorithm gives a computationally efficient method performing the feature extraction from multi-frequency eddy current (MFEC) data. The algorithm has been applied to both, simulated data using finite element method (FEM) and experimental MFEC field data. The results indicate that independent component analysis (ICA) is a feasible approach for extracting signals from flaws in steam generator tubes, even when the flaw is close to support plates. The algorithm can also be used to enhance the flaw signal in the presence of noise.

6.2. Future Work

Future work will focus on a study of the following issues.

- Test the algorithm on more exhaustive data set.
- More robust and automated method to pick up the defect signal from the output of ICA algorithm is required.
- The performance of ICA algorithm depends largely on the linearity of MFECT data. It is assumed that the observed MFECT data is a linear mixture of the source signals. The validity of this assumption at different frequencies and its defect on

the result should be further studied. An alternate approach is to develop ICA model to solve the nonlinear mixture problem.

- ICA is a statistical method to extract source signal using a method that minimizes gaussianity. Due to this property, ICA cannot be used to extract a signal that has Gaussian distribution. In this paper, Gaussian noise signal is extracted using residual theory. However, this is useful when only one Gaussian noise component is present in the mixture. In this thesis, only one Gaussian measurement noise is assumed to be present in the MFECT data. However, in order to model variation in lift-off and surface roughness, which usually have Gaussian distributions additional work need to be done. A simple approach is to eliminate noise signal before applying ICA algorithm.

References

[1] Kenneth. C. Weston, "Energy Conversion: Chapter 10. Nuclear Power Plants", e-book, available at http://www.personal.utulsa.edu/~kenneth-weston/"

[2] S. Udpa, L. Udpa, "Eddy Current Nondestructive Evaluation" in Wiley Encyclopedia of Electrical and Electronics Engineering, edited by John G. Webster, Wiley-Interscience Publication, New York, 1999,Vol. 6.

[3] S.P. Sullivan, V.S. Cecco, L.S. Obrutsky, J.R. Lakhan and A.H. Park., "Validating Eddy Current Array Probes for Inspecting Steam Generator Tubes", European Commission JRC, Institute for Advanced Materials, 1998 January, Vol.3, No.1

[4] K. Arunchalam, P. Ramuhali, L. Udpa, S. Udpa, "Nonlinear Mixing Algorithm For Suppression of TSP Signals In Bobbin Coil Eddy Current Data," *Review of Progress of Progress in QNDE*, Vol. 21, D. O. Thompson and D. E. Chimenti (Eds.), American Institute of Physics, 2002, pp.631-638.

[5] C. Jutten and J. Herault, "Blind separation of sources, part I : An adaptive algorithm based on neuromimetic architecture," *Signal Processing* 24, 1~10, 1991.

[6] C. Jutten, J. Herault and P. Comon, "Blind separation of sources, Part II : Problem statement," Signal Processing, Vol. 24, 11~20, 1991.

[7] A. J. Bell and T. J. Sejnowski, "An Information-Maximization Approach to Blind Separation and Blind Deconvolution," *Neural Computation* 7, 1129~1159, 1995.

[8] S. Amari, "Narural Gradient works efficiently in learning," *Neural Computation*, 10, 251~276, 1997.

[9] Te-Won Lee, M. Girolami and T. J. Sejnowski, "Independent Component Analysis using an Extended Infomax Algorithm for Mixed Sub-Gaussian and Super Gaussian Sources," 4th Joint Synposium on Neural Computation, 7, 132-140, Institute for Neural Computation, 1997.

[10] A. Hyvärinen, "Fast and Robust Fixed-Point Algorithms for Independent Component Analysis," *IEEE Trans. on Neural Computation*, 10(3):626-634, 1995.

[11] A. Hyvärinen and E. Oja, "A fast fixed-point algorithm for independent component analysis," *IEEE Trans. on Neural Computation*, 9(7):1483-1492, 1997.

[12] Udpa, L. "Imaging of Electromagnetic NDT Phenomena." Ph.D. Dissertation, Colorado State University, Ft. Collins, 1983.

[13] S.N. Rajesh, "Probability of detection models for eddy current NDE method."

Master Thesis, Ames, 1993.

[14] Cecco V.S. and Van Drunen, "Recognizing the Scope of Eddy Current Testing", in Research Techniaues in Nondestructive Testing, Vol. 8, 1985, pp 269-301, ed. by R.S. Sharpe, Academic Press.

[15] Mundis, J. A. and DeYoung, G. W. "Solution to NDE Problems in PWR Steam Generators – An Overview." Quantitative NDE in the Nuclear Industry. Edited by R.B. Clough. Metals Park, Ohio: American Society for Metals, 1983. P.93-98.

[16] Brown, S. D. "Multifrequency/Multiparameter Eddy Current Steam Generator NDE." Quantitative NDE in the Nuclear Industry. Edited by R.B. Clough, Metals Park, Ohio: American Society for Metals, 1983. p.99-105.

[17] Smith, J., Dodd, C., and Chitwood, L. "Multifrequency Eddy Current Examination of Seam Weld in Stell Sheath." Materials Evaluation Vol.43. November, 1985. p. 1566-1572.

[18] Libby, H. L. Introduction to Electromagnetic Nondestructive Test Models. New York: John Wiley and Sons, Inc., 1971.

[19] Saglio, R. and Pigeon, M. "Concepts of Multifrequency Eddy Current Testing." Electromagnetic Testing. Vol. 4, 2nd ed. Edited by P. McIntire, R. McMaster. Columbus, Ohio: American Society for Nondestructive testing, 1986. p.592-605.

[20] Solete, J., Udpa, L., and Lord. W. "Multifrequency Eddy Current Testing of Steam Generator Tubes Using Optimal Affine Transform." Review of Progress in Quantitative Nondestructive Evaluation, Vol. 7A. Edited by D.O. Thompson and D.E. Chimenti. New York: Plenum Press, 1988. p.821-830.

[21] Libby, H. L. "Eddy Current Test for Tubing Flaws in Support Regions." Research Techniques in Nondestructive Testing, Vol. II. Edited by R.S. Sharpe. London: Academic Press, 1973. p151-184.

[22] C.L. Owsley, "A Multifrequency Eddy Current NDE System." Master Thesis, Ames, 1996.

[23] A. Leon-Garcia, "Probability and Random Processes for Electrical Engineering," Addison Wesley, 2nd edition,

[24] J.H. Wilkinson, The Algebraic Eigenvalue Problem, Oxford University Press, Oxford, 1965.

[25] M. Kendall and A. Stuart, The advanced theory of statistics, Mcgraw Hill, 1969.

[26] P. Comon, "Independent component analysis - a new concept", *Signal Processing*,

36:287-314, 1994.

[27] M.C. Jones and R. Sibson, "What is projection pursuit?", *J. of the Royal Statistical Society, ser. A*, 150:1-36, 1987.

[28] A. Hyvärinen. New approximations of differential entropy for independent component analysis and projection pursuit. In advances in Neural Information Processing Systems, Vol. 10, p 273-279, MIT Press, 1998.

[29] G. Arfken, Mathematical Method for Physicists, 3rd edition, American Press, 1985.

[30] L. V. Kantorovich and G.P. Akilov, Functional Analysis in Normed Spaces, Pergamon Press, Elmsford, New York, 1964.

[31] J. Karhunen, E. Oja, L. Wang, R. Vigario, and J. Joutsensalo. "A class of neural networks for independent component analysis", *IEEE Trans. on Neural Networks*, 8(3):486-504, 1997.

[32] A. Hyvärinen, "One-unit contrast functions for independent component analysis: A statistical analysis", In *Neural Networks for Signal Processing VII (Proc. IEEE Workshop on Neural Networks for Signal Processing)*, pages 388-397, Amelia Island, Florida, 1997.

[33] M. Kendall and A. Stuart, "*The Advanced Theory of Statistics*", Charles Griffin & Company, 1958.

[34] The Eddy Current Simulation with Finite Element Method in MATLAB code. Available at "http://www.egr.msu.edu/~ zengzhiw/".

[35] Lord, W. and Palanisamy, R. "Magnetic Probe Inspection of steam Generator Tubing." Materials Evaluation, Vol. 38, No. 5, May 1980, p478-485

[36] J. Freund, Mathematical statistics, Prentice Hall, Upper Saddle River, New Jersey, six edition, 1999.